



## Performance of interFoam on the simulation of progressive waves

Larsen, Bjarke Eltard; Fuhrman, David R.; Roenby, Johan

*Published in:*  
Coastal Engineering Journal

*Link to article, DOI:*  
[10.1080/21664250.2019.1609713](https://doi.org/10.1080/21664250.2019.1609713)

*Publication date:*  
2019

*Document Version*  
Peer reviewed version

[Link back to DTU Orbit](#)

*Citation (APA):*  
Larsen, B. E., Fuhrman, D. R., & Roenby, J. (2019). Performance of interFoam on the simulation of progressive waves. *Coastal Engineering Journal*, 61(3), 380-400. <https://doi.org/10.1080/21664250.2019.1609713>

---

### General rights

Copyright and moral rights for the publications made accessible in the public portal are retained by the authors and/or other copyright owners and it is a condition of accessing publications that users recognise and abide by the legal requirements associated with these rights.

- Users may download and print one copy of any publication from the public portal for the purpose of private study or research.
- You may not further distribute the material or use it for any profit-making activity or commercial gain
- You may freely distribute the URL identifying the publication in the public portal

If you believe that this document breaches copyright please contact us providing details, and we will remove access to the work immediately and investigate your claim.

## Performance of `interFoam` on the simulation of progressive waves

Bjarke Eltard Larsen<sup>a</sup>, David R. Fuhrman<sup>a</sup> and Johan Roenby<sup>b</sup>

<sup>a</sup>Technical University of Denmark, Department of Mechanical Engineering, Section of Fluid Mechanics, Coastal and Maritime Engineering, DK-2800 Kgs. Lyngby, Denmark; <sup>b</sup>DHI, Department of Port & Offshore Technology, Agern Allé 5, 2970 Hørsholm

### ARTICLE HISTORY

Compiled May 1, 2019

### ABSTRACT

The performance of `interFoam` (a widely-used solver within the popular open source CFD package `OpenFOAM`®) in simulating the propagation of a nonlinear (stream function solution) regular wave is investigated in this work, with the aim of systematically documenting its accuracy. It is demonstrated that over time there is a tendency for surface elevations to increase, wiggles to appear in the free surface, and crest velocities to become (severely) over estimated. It is shown that increasing the temporal and spatial resolution can mitigate these undesirable effects, but that a relatively small Courant number is required and fine discretization is needed, indicating that many past simulations have not converged. It is further demonstrated that the choice of discretization schemes and solver settings (often treated as a "black box" by users) can have a major impact on the results. This impact is documented, and it is shown that obtaining a "diffusive balance" is crucial to accurately propagate a surface wave over long distances without requiring exceedingly high temporal and spatial resolutions. Finally, the new code `isoAdvector` is compared to `interFoam`, which is demonstrated to produce comparably accurate results, while maintaining a sharper surface. It is hoped that the systematic documentation of the performance of the `interFoam` solver will enable its more accurate and optimal use, as well as increase awareness of potential shortcomings, by CFD researchers interested in the general CFD simulation of free surface waves.

### KEYWORDS

`interFoam`, waves, discretization practises, `isoAdvector`

## 1. Introduction

As a tool to simulate waves `interFoam`, in the widely-used CFD package `OpenFOAM`® (or other solvers build on `interFoam`, e.g. `waves2Foam` developed by Jacobsen et al. (2012)) are becoming increasingly popular. As examples, `interFoam` has been utilized to simulate breaking waves by e.g. Jacobsen et al. (2012); Brown et al. (2016); Jacobsen et al. (2014); Lupieri and Contento (2015); Higuera et al. (2013). It has also been used to simulate wave-structure interaction by e.g. Higuera et al. (2013); Chen et al. (2014); Paulsen et al. (2014); Hu et al. (2016); Jacobsen et al. (2015); Schmitt and Elsaesser (2015).

Wave breaking and wave-structure interaction are both very complex phenomena, but `interFoam` has also been utilized to simulate more simple cases, such as the pro-

gression of a solitary wave by Wroniszewski et al. (2014), which was suggested as a benchmark to compare to other CFD codes. The study by Wroniszewski et al. (2014) highlighted a problem, that to our knowledge, has gone largely unnoticed in the formal journal literature, namely that the velocity at the crest of the wave is over-predicted relative to the analytical solutions. This was also highlighted in conference paper Roenby et al. (2017), the MSc thesis of Afshar (2010) and the PhD thesis Tomaselli (2016). A second problem was highlighted in the study by Paulsen et al. (2014), where it was shown that `interFoam` is not capable of maintaining a constant wave height for long propagation distances. They also mentioned, though not going into great detail, that the choice of convection scheme affected this behaviour. The choice of convection scheme was also briefly touched upon by Wroniszewski et al. (2014), who, like Paulsen et al. (2014), utilized an upwind scheme, chosen for stability reasons. These two studies thus hinted at the importance of discretization practises when using `interFoam` to simulate waves, but no further discussion of this was made. A third (again not well described in the literature) problem is the appearance of wiggles in the air-water interface, as documented by Afshar (2010). A fourth problem, which has received considerable attention (though not in the context of waves), is the growth of spurious velocities in low density fluid near the interface; see e.g. Francois et al. (2006); Meier et al. (2002); Rudman (1997); Popinet and Zaleski (1999); Shirani et al. (2005); Menard et al. (2007); Tanguy et al. (2007); Galusinski and Vigneaux (2008); Hysing (2006). The previous mentioned studies all related the growth of spurious velocities to the surface tension. More recently, however, it should be noted that Vukcevic (2016); Vukcevic et al. (2016, 2017); Wemmenhove et al. (2015) demonstrated development of spurious velocities in situations without surface tension.

While a benchmark case as presented in Wroniszewski et al. (2014) is, in principal, a good idea many relevant details of the `interFoam` setup were not presented, and this is typically the case in many of the previous mentioned studies. Such details are quite important, at least from the perspective of benchmarking, as it turns out that the performance of `interFoam` is quite sensitive to the setup (briefly touched upon in Paulsen et al. (2014) and Wroniszewski et al. (2014) in the choice of convection scheme). Hence, prior to benchmarking `interFoam` or other CFD solvers, it is imperative that an "optimal" (or at least reasonably so) settings be known and utilized.

As the intended audience of the present paper is `OpenFOAM`® users, a working knowledge of this software is assumed throughout. To shed light on the general CFD simulation of surface gravity waves, the present study will systematically investigate the performance of `interFoam` on a canonical case involving a simple, intermediately deep, progressive regular wave train. It will demonstrate that taking `interFoam` "out of the box," i.e. utilizing the standard setup from one of the popular tutorials, will yield quite poor results (This could be expected since the `OpenFOAM`® tutorials are designed to run first and foremost stably rather than accurately). After showing the default performance of `interFoam` the sensitivity of `interFoam` to different settings will be investigated. First, a standard sensitive analysis is conducted with respect to the Courant number and mesh resolution. This is done specifically to highlight that commonly-used Courant numbers may not be sufficiently small to accurately simulate gravity waves, indicating that many past results might not have converged. Then, utilizing a lower Courant number, different `interFoam` settings will be systematically tested to demonstrate the importance of discretization considerations when simulating waves and finally the settings will be combined to form a reasonably optimal set up. The recently developed code `isoAdvector` will finally be coupled with `interFoam`, and the performance of `interFoam` (utilizing `isoAdvector` instead of `MULES`) will be

62 compared to the performance of the standard `interFoam` solver.

## 63 2. Model description

### 64 2.1. Hydrodynamics

65 The flow is simulated by solving the continuity equation coupled with momentum  
66 equations, respectively given in (1) and (2):

$$\frac{\partial u_i}{\partial x_i} = 0, \quad (1)$$

67

$$\frac{\partial \rho u_i}{\partial t} + u_j \frac{\partial \rho u_i}{\partial x_j} = -\frac{\partial p^*}{\partial x_i} - g_j x_j \frac{\partial \rho}{\partial x_i} + \frac{\partial}{\partial x_j} (2\mu S_{ij}) + \sigma_T \kappa \frac{\partial \alpha}{\partial x_i}, \quad (2)$$

68 Here  $u_i$  are the mean components of the velocities,  $x_i$  are the Cartesian coordinates,  
69  $\rho$  is the fluid density (which takes the constant value  $\rho_{\text{water}}$  in the water and jumps at  
70 the interface to the constant value  $\rho_{\text{air}}$  in the air phase),  $p^*$  is the pressure minus the  
71 hydrostatic potential  $\rho g_j x_j$ ,  $g_j$  is the gravitational acceleration,  $\mu = \rho \nu$  is the dynamic  
72 molecular viscosity ( $\nu$  being the kinematic viscosity), and  $S_{ij}$  is the mean strain rate  
73 tensor given by

$$S_{ij} = \frac{1}{2} \left( \frac{\partial u_i}{\partial x_j} + \frac{\partial u_j}{\partial x_i} \right). \quad (3)$$

74 The last term in equation (2) accounts for the effect of surface tension,  $\sigma_T$ , where  
75  $\kappa$  is the local surface curvature and  $\alpha$  is the so-called indicator field introduced for  
76 convenience, which takes value 0 in air and 1 in water. It can be defined in terms of  
77 the density as

$$\alpha = \frac{\rho - \rho_{\text{air}}}{\rho_{\text{water}} - \rho_{\text{air}}}. \quad (4)$$

78 We assume that any intrinsic fluid property,  $\Phi$ , can be expressed in terms of  $\alpha$  as

$$\Phi = \alpha \Phi_{\text{water}} + (1 - \alpha) \Phi_{\text{air}}. \quad (5)$$

79 The evolution of  $\alpha$  is determined by the continuity equation, which in terms of  $\alpha$  reads

$$\frac{\partial \alpha}{\partial t} + \frac{\partial \alpha u_j}{\partial x_j} = 0. \quad (6)$$

80 In `interFoam` the numerical challenge of keeping the interface sharp is addressed using  
81 a numerical interface compression method and limiting the phase fluxes based on the  
82 "Multidimensional universal limiter with explicit solution" (`MULES`) limiter. Numerical  
83 interface compression is obtained by adding a purely heuristic term to equation (6),  
84 such that it attains the form

$$\frac{\partial \alpha}{\partial t} + \frac{\partial \alpha u_j}{\partial x_j} + \frac{\partial}{\partial x_j} (\alpha(1 - \alpha)u_j^r) = 0. \quad (7)$$

85 Here  $u_j^r$  is a modelled relative velocity used to compress the interface and is given by

$$u_j^r = \min \left( \frac{c_\alpha |F_f|}{|s_f|}, \max \left[ \frac{|F_f|}{|s_f|} \right] \right) n_{f,j} \quad (8)$$

86 where  $c_\alpha$  is a user defined value that determines the strength of the compression,  $F_f$  is  
87 the face flux,  $n_{f,j}$  is the  $j$ 'th component of the interface normal and  $s_f$  is the face area  
88 vector normal to the face pointing out of the cell. For more details on the numerical  
89 implementation, the reader is referred to Deshpande et al. (2012).

90 All simulations are performed utilizing OpenFOAM® version `foam-extend 3.2`. The  
91 authors are aware of a "new" MULES algorithm (not present in the extend versions)  
92 in newer versions from OpenFOAM-2.3.0, and also of the new commit support for  
93 Crank-Nicolson on the time integration of  $\alpha$ . Therefore the base case to be presented  
94 later, was also simulated utilizing a newer version of the standard OpenFOAM®, namely  
95 OpenFOAM-3.0.1. We were unable to produce significantly different results with these  
96 newer versions as compared to our simulations with `foam-extend 3.2`, hence the base  
97 performance demonstrated in what follows is likewise expected to be representative of  
98 newer versions.

## 99 2.2. *Boundary and initial conditions*

100 For this study a simple base case of a regular propagating wave will be simulated  
101 with various numerical settings. The quality of the simulated wave will be assessed  
102 through comparison with the analytical solution in terms of surface elevations and  
103 velocity profiles. We use a so-called stream function wave from Rienecker and Fenton  
104 (1981), initialized with `waves2Foam` developed by Jacobsen et al. (2012), with a period  
105  $T = 2$  s and wave height  $H = 0.125$  m at a water depth of  $h = 0.4$  m. This gives  
106  $kh = 0.66$  and  $H/h = 0.31$ , which indicates that the simulated wave is non-linear and  
107 at intermediate depth, with  $k$  being the wave number. The stream function solution can  
108 be considered as a numerically exact wave solution based on nonlinear potential flow  
109 equations. The properties have been selected to correspond to the incoming wave in the  
110 well-known spilling breaker experiment of Ting and Kirby (1994). For all simulations  
111 the wave will be propagated through a domain which is exactly one wave length long  
112 and two water depths high with cyclic periodic boundary conditions on the sides.  
113 Unless stated otherwise the domain is discretised into cells having an aspect ratio of  
114 1 with the number of cells per wave height  $N = H/\Delta y = 12.5$ , resulting in cells with  
115  $\Delta x = \Delta y = 0.01$  m. This results in a two dimensional domain with  $379 \times 80$  cells. At  
116 the bed a slip condition is utilized for the velocities in accordance with potential flow  
117 theory. At the top the `pressureInletOutletVelocity` is used. This means that there  
118 is a zero gradient condition except on the tangential component which has a value of  
119 zero. For  $p^*$  zero-gradient conditions are used for the bed and the periodic boundaries  
120 whereas the top used a `totalPressure` condition with `p0=0`. Note that this setup  
121 was also used in the study by Larsen and Fuhrman (2018) in the testing of their new  
122 turbulence model.

### 123 3. interFoam settings

124 In this section the default numerical settings for our simulations, as well as a general  
125 description of OpenFOAM®’s discretization practices, are presented. Our base numerical  
126 settings will be those found in the popular `damBreak` tutorial shipped with  
127 `foam-extend-3.2`. With this starting point we will change various settings to investigate  
128 their effect on the quality of the numerical solution. More specifically, we copy the  
129 `controlDict`, `fvSchemes` and `fvSolution` files directly from the `damBreak` tutorial. In  
130 the `constant` directory the mesh and the physical parameters of the case are specified:  
131  $\rho_{\text{water}}=1000 \text{ kg/m}^3$ ,  $\rho_{\text{air}} = 1.2 \text{ kg/m}^3$ ,  $\nu_{\text{water}} = 1 \cdot 10^{-6} \text{ m}^2/\text{s}$ ,  $\nu_{\text{air}} = 1.45 \cdot 10^{-5} \text{ m}^2/\text{s}$ ,  
132 and  $\sigma_T = 0.0 \text{ N/m}$  (i.e. no surface tension). We note that the analytic stream function  
133 solution does not take into account the presence of air, nor the effect of viscosity or  
134 surface tension. With the chosen wave parameters and boundary conditions (e.g. no  
135 slip at the bed) the physics are dominated by inertia and gravity. With a density ratio  
136 of  $\rho_{\text{water}}/\rho_{\text{air}} \sim 833$ , the air will behave like a “slave fluid” moving passively out of the  
137 way for the water close to the surface. To confirm the insignificance of the physical  
138 viscosity in our setup, we have compared simulations with these set to their physical  
139 values and to  $\nu = 1 \cdot 10^{-16} \text{ m}^2/\text{s}$ , and confirmed that this had no effect on our results.  
140 We have also performed simulations with  $\rho_{\text{air}} = 0.1 \text{ kg/m}^3$  and  $\rho_{\text{air}} = 10 \text{ kg/m}^3$ . This  
141 had almost no effect in the short term, but had some effect for long propagation distances.  
142 Increasing the density made the air behave less like a “slave fluid” and slowed  
143 the propagation of the wave. Decreasing the density created larger air velocities, but  
144 did not alter the wave kinematics significantly. We have confirmed that switching the  
145 surface tension between zero and its physical value ( $\sigma_T = 0.07 \text{ N/m}$ ) had next to  
146 no effect on our simulation results, as expected in the gravity wave regime. Finally,  
147 the simulations are performed without turbulence, as the results are intended to be  
148 compared with the idealized stream function (potential flow) solution.

149 The OpenFOAM® case setup is contained in a file called `controlDict` which, among  
150 others things, controls the time stepping method. The schemes used to discretize the  
151 different terms in the governing equations are specified in the `fvSchemes` file, and the  
152 file `fvSolution` contains various settings for the linear solvers and for the solution  
153 algorithm. In Table 1 the essential parameters for the base set up from these three  
154 files are indicated. The most important details of the scheme and solver choices presented  
155 in Table 1 will be described in the following. For descriptions of the remaining  
156 settings, the reader is referred to the OpenFOAM® user guide and programmers guides  
157 in Greenshields (2015, 2016).

#### 158 3.1. *controlDict*

159 In this subsection the most important `controlDict` settings are presented. The time  
160 step can be specified either as `fixed`, such that the user defines the size of the time step,  
161 or as `adjustable`. In the latter case the time step is adjusted such that a maximum  
162 Courant number  $Co = u_i \Delta t / \Delta x_i$  or a maximum `AlphaCo` (The Courant number in  
163 interface cells) is maintained at all times. Since these two for the remainder of this  
164 study are kept equal it is  $Co$  that controls the time step. In the `damBreak` tutorial an  
165 adjustable time step is used with  $Co = 0.5$ , hence this value will be utilized initially.

**Table 1.** Base setup from the damBreak tutorial

controlDict	Scheme/Value
adjustTimeStep	true
maxCo	0.5
maxAlphaCo	0.5
fvSchemes	
ddt	Euler
grad	Gauss Linear
div(rho*phi,U)	Gauss LimitedLinearV 1
div(phi,alpha1)	Gauss VanLeer01
div(phirb,alpha1)	Gauss interfaceCompression
laplacian	Gauss linear corrected
interpolation	linear
snGrad	corrected
fvSolution	
pcorr(solver,prec,tol,relTol)	PCG, DIC, 1e-10, 0
pd(solver,prec,tol,relTol)	PCG, DIC, 1e-07, 0.05
pdFinal(solver,prec,tol,relTol)	PCG, DIC, 1e-07, 0
U(solver,prec,tol,relTol)	PBiCG, DILU, 1e-06, 0
cAlpha	1
momentumPredictor	yes
nOuterCorrectors	1
nCorrectors	4
nNonOrthogonalCorrectors	0
nAlphaCorr	1
nAlphaSubCycles	2

### 166 3.2. *fvSchemes*

167 In this subsection some of the discretisation schemes are presented to aid in the  
168 understanding of the forthcoming analysis. The `ddt` scheme specifies how the time  
169 derivative  $\partial/\partial t$  is handled in the momentum equations. Available in `OpenFOAM` are:  
170 `steadyState`, `Euler`, `Backwards` and `CrankNicolson`. In this study, `steadyState` is  
171 naturally disregarded as the simulations are unsteady. The `Euler` scheme corresponds  
172 to the first-order backward implicit Euler scheme, whereas `Backward` corresponds to  
173 a second-order, `OpenFOAM` implemented time discretization scheme, which utilizes the  
174 current and two previous time steps. The `CrankNicolson` (CN) scheme includes a  
175 blending factor  $\psi$ , where  $\psi = 1$  corresponds to pure (second-order accurate) CN and  
176  $\psi = 0$  corresponds to pure `Euler`. This blending factor is introduced to give increased  
177 stability and robustness to the CN scheme.

178 In the finite volume approach used in `OpenFOAM`, the convective terms in the mass  
179 (7) and momentum (2) equations are integrated over a control volume, and afterwards  
180 the Gauss theorem is applied to convert the integral into a surface integral:

$$\int_V \nabla \cdot (\phi u) dV = \oint_S \phi (n \cdot u) dS \approx \sum_f \phi_f F_f, \quad (9)$$

181 where  $\phi(x, t)$  is the field variable,  $\phi_f$  is an approximation of the face averaged field  
182 value.  $\phi_f$  can be determined by interpolation, e.g. using central or upwind differencing.  
183 Central differencing schemes are second order accurate, but can cause oscillations in

184 the solution. Upwind differencing schemes are first order accurate, cause no oscillations,  
 185 but can be very diffusive.

186 `OpenFOAM` includes a variety of total variation diminishing (TVD) and normalized  
 187 variable diagram (NVD) schemes aimed at achieving good accuracy while maintaining  
 188 boundedness. TVD schemes calculate the face value  $\phi_f$  by utilizing combined upwind  
 189 and central differencing schemes according to

$$\phi_f = (1 - \Gamma)\phi_{f,UD} + \Gamma\phi_{f,CD0} \quad (10)$$

190 where  $\phi_{f,UD}$  is the upwind estimate of  $\phi_f$ ,  $\phi_{f,CD}$  is the central differencing estimate of  
 191  $\phi_f$ .  $\Gamma$  is a blending factor, which is a function of the variable  $r$  representing the ratio  
 192 of successive gradients,

$$r = 2 \frac{d \cdot (\nabla \phi)_P}{\phi_N - \phi_P}. \quad (11)$$

193 Here  $d$  is the vector connecting the cell centre  $P$  and the neighbour cell centre  $N$ .  
 194 In NVD-type schemes the limiter is formulated in a slightly different way. In the  
 195 `damBreak` tutorial base setup the TVD scheme is utilized by specifying the key-  
 196 word `limitedLinearV 1` for the momentum flux, `div(rho*phi,U)`, and `vanLeer01`  
 197 for the mass flux, `div(phi,alpha1)`, where the keyword `phi` means face flux. With  
 198 the `limitedLinear` scheme  $\Gamma = \max[\min(2r/k, 1), 0]$ , where  $k$  is an input given by  
 199 the user, in this case  $k = 1$ . When using the scheme for vector fields a "V" can be  
 200 added to the TVD schemes, which changes the calculation of  $r$  to take into account  
 201 the direction of the steepest gradients. The `vanLeer` scheme calculates the blending  
 202 factor as  $\Gamma = (r + |r|)/(1 + |r|)$ . The `01` added after the TVD scheme name means  
 203 that  $\Gamma$  is set to zero if it goes out of the bounds 0 and 1, thus going to a pure upwind  
 204 scheme to stabilize the solution. The other available TVD/NVD schemes differ in their  
 205 definition of  $\Gamma$  and resulting degree of diffusivity. Since  $r$  depends on the numerically  
 206 calculated gradient of  $\phi$ , the choice of gradient scheme can also play an important role.  
 207 In general the gradients are calculated utilizing a Gauss linear scheme, but this might  
 208 lead to unbounded face values, and therefore gradient limiting can be applied. As an  
 209 example the gradient scheme can be specified as `Gauss faceMDLimited`. The keyword  
 210 `face` or `cell` specifies whether the gradient should be limited base on cell values or  
 211 face values and the keyword `MD` specifies that it should be the gradient normal to the  
 212 faces. In addition to the linear choice of gradient schemes there also exists a least  
 213 square scheme as well as a fourth order scheme.

214 The `laplacian` scheme specifies how the Laplacian in the pressure correction equa-  
 215 tion within the PISO algorithm, as well the third term on the right hand side of  
 216 equation (2), should be discretized. It requires both an interpolation scheme for the  
 217 dynamic viscosity,  $\mu$ , and a surface normal gradient scheme `snGrad` for  $\nabla u$ . Often  
 218 a `linear` scheme is used for the interpolation of  $\mu$  and the proper choice of surface  
 219 normal gradient scheme depends on the orthogonality of the mesh. Besides being used  
 220 in the Laplacian, the `snGrad` is also used to evaluate the second and fourth term on  
 221 the right hand side of equation (2). Often a linear scheme will be used, with or with-  
 222 out orthogonality correction. Another option is to use a fourth order surface normal  
 223 gradient approximation. Finally, the interpolation scheme determines how values are  
 224 interpolated from cell centres to face centres.

### 225 3.3. *fvSolution*

226 In the `fvSolutions` file the iterative solvers, solution tolerances and algorithm settings  
227 are specified. The available iterative solvers are preconditioned (bi-)conjugate gradient  
228 solvers denoted `PCG/PBiCG`, a `smoothSolver`, generalised geometric-algebraic multi-  
229 grid, denoted `GAMG`, and a `diagonal` solver. Each solver can be applied with different  
230 preconditioners and the smooth solver also has several smoothing options. The `GAMG`  
231 solver works by generating a quick solution on a coarse mesh consisting of agglomerated  
232 cells, and then mapping this solution as the initial guess on finer meshes to finally  
233 obtain an accurate solution on the simulation mesh. The different preconditioners and  
234 smoothers will not be discussed here, but Greenshields (2015, 2016) can be consulted  
235 for additional details.

236 In addition to the solver choices the `PISO`, `PIMPLE` and `SIMPLE` controls are also given  
237 in the `fvSolution` file. The `cAlpha` keyword controls the magnitude of the numerical  
238 interface compression term in equation (7). `cAlpha` is usually set to 1 corresponding  
239 to a “compression velocity” of the same size as the flow velocity at the interface. The  
240 `momentumPredictor` is a switch specifying enabling activation/deactivation of the pre-  
241 dictor step in the `PISO` algorithm. The parameter, `nOuterCorrectors` is the number of  
242 outer correctors used by the `PIMPLE` algorithm and specifies how many times the entire  
243 system of equations should be solved within one time step. To run the solver in “`PISO`  
244 mode” we set `nOuterCorrectors` to 1. The parameter `nCorrectors` is the number  
245 of pressure corrector iterations in the `PISO` loop. The parameter `nAlphaSubCycles`  
246 enables splitting of the time step into `nAlphaSubCycles` in the solution of the  $\alpha$  equa-  
247 tion (7). Finally, the parameter `nAlphaCorr`, specifies how many times the `alpha` field  
248 should be solved within a time step, meaning that first the `alpha` field is solved for,  
249 and this new solution is then used in solving for the `alpha` field again.

## 250 4. Results and discussion

251 In this section the simulated results involving the propagation of the regular stream  
252 function wave will be presented and discussed for various settings.

### 253 4.1. *Performance of interFoam utilizing the damBreak settings*

254 First, the “default” performance of `interFoam` in the progression of the stream function  
255 wave is presented, utilizing the settings from the `damBreak` tutorial. The setup utilized  
256 here will be considered as the base setup, and the remainder of the simulations in this  
257 study will utilize this base setup with minor adjustments.

258 Starting from the analytical stream function solution imposed as an initial condi-  
259 tion (utilizing the `waves2Foam` toolbox of Jacobsen et al. (2012)), the simulation is  
260 performed for 200 s (corresponding to 100 periods). This is sufficiently long to high-  
261 light certain strengths and problems of `interFoam`. Results are sampled at the cyclic  
262 boundary 20 times per period. In Figure 1 the surface elevation time series is shown.  
263 Quite noticeably, even though the depth is constant, the wave height immediately  
264 starts to increase, and this continues until the wave at some point (approximately  
265 at  $t = 20T$ ) breaks. This rather surprising result demonstrates the potentially poor  
266 performance of `interFoam`, as the wave does not come close to maintaining a con-  
267 stant form. A similar result has been shown in Afshar (2010). A feature that seems  
268 to contribute, though is not solely responsible for, the un-physical steepening of the

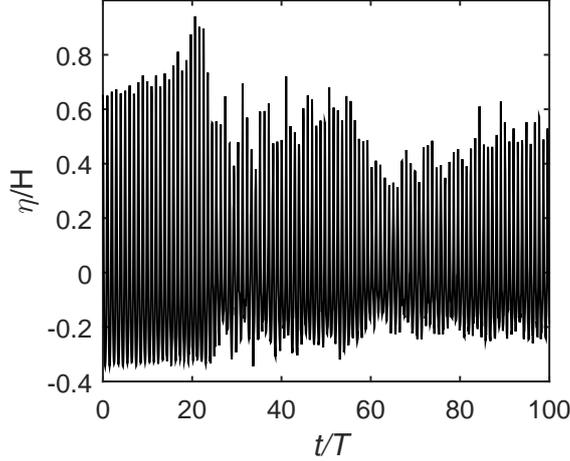


**Figure 1.** Surface elevation for the propagating wave utilizing the damBreak setup

269 wave, is small "wiggles" on the interface. These are illustrated in Figure 2 where a  
 270 snapshot of the wave is seen after approximately five and 16 periods. The vertical  
 271 axes are exaggerated to highlight the presence of the wiggles. As the wave propagates  
 272 these wiggles emerge, continue to grow and sometimes merge, hence contributing to  
 273 the steepening of the wave, which ultimately breaks. The cause of the wiggle feature  
 274 will be discussed in Section 4.4.

275 While propagating, in addition to steepening, the celerity is also increasing com-  
 276 pared to the analytical stream function solution, resulting in a phase error. To demon-  
 277 strate this the surface elevation for the first 20 periods is compared with the stream  
 278 function solution in Figure 3. Here it is quite evident that significant phase errors occur  
 279 after approximately propagating for 10 periods, where the simulated results start to  
 280 lead the analytical solution. This corresponds approximately to the time where over-  
 281 steepening is apparent, hence the phase error may be attributed to the un-physical  
 282 increase in the nonlinearity of the wave.

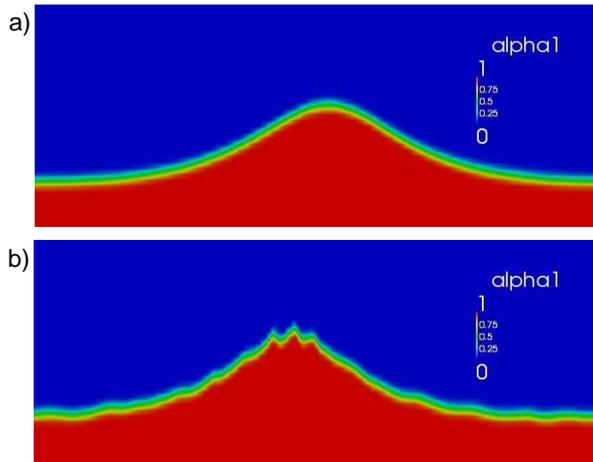


**Figure 2.** Snapshot at a)  $t = 5.5T$  and b)  $t = 16.25T$ , illustrating the appearance of small wiggles in the crest after sufficiently long propagation

283 Also of great interest is the velocity profile beneath the propagating wave, as velocity  
 284 kinematics often form the basis for force calculations on coastal or offshore structures,

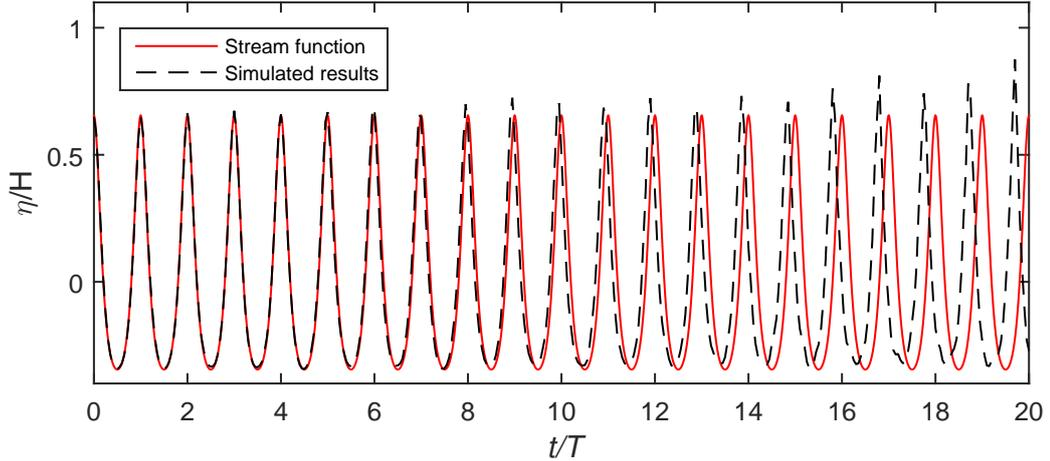


**Figure 3.** Surface elevation for the propagating wave utilizing the damBreak setup

285 while also influencing e.g. bed shear stresses and hence sediment transport predictions  
 286 (in simulations where the boundary layer is also resolved). In Figure 4 the velocity  
 287 profile directly beneath the crest of the wave after five periods is shown together with  
 288 the analytical stream function solution. It should be noted that the velocity here, and  
 289 in future results, is taken as  $U = u_1\alpha$ , and it is only shown from the bed until the  
 290 height where it reaches its maximum value. This is done to capture the velocity all  
 291 the way to the crest of the wave and not merely to a predefined height (as just shown,  
 292 the wave height increases). Furthermore, this formulation also includes the velocities  
 293 at cells containing a mixture of air and water, which is desirable, as some diffusion of  
 294 the interface is seen.

295 As seen in Figure 4, the velocity beneath the crest is underestimated close to the  
 296 bed and, especially near the free surface, is severely overestimated. This is despite the  
 297 fact that the wave has still reasonably maintained its shape up to this time, see Figure  
 298 2a and 3. This over-predicted crest velocity, in addition to the steepening of the wave,  
 299 also likely contributes to the wave breaking. The overestimation of crest velocities in  
 300 regular waves by `interFoam` has, to our knowledge, gone almost un-recognized in the  
 301 journal literature. It is recorded in Wroniszewski et al. (2014) in the propagation of a  
 302 solitary wave and in Roenby et al. (2017) as well as in the MSc thesis of Afshar (2010)  
 303 and the PhD thesis of Tomaselli (2016). The overestimation of the crest velocity is  
 304 believed to arise from an imbalance in the discretized momentum equation near the  
 305 interface. As the wave propagates the increase in crest velocity becomes continually  
 306 worse, and in addition to the imbalance in the momentum equation near the free  
 307 surface, the steepening of the wave also contributes to this increase.

308 Finally, though not shown herein for brevity, we note that regions of high air ve-  
 309 locities were seen to develop just above the free surface and in the mixture cells. Such  
 310 spurious velocities have elsewhere been attributed to surface tension effects, see e.g.  
 311 Deshpande et al. (2012), but the spurious velocities found in these simulation are  
 312 clearly of a different nature as the surface tension is turned off. The main challenge  
 313 leading to this behavior is that when the water/air density ratio is high, even small  
 314 erroneous transfers of momentum across the interface from the heavy to the light fluid  
 315 will cause a large acceleration of the light fluid, as also discussed by Vukcevic (2016);  
 316 Vukcevic et al. (2016); Wemmenhove et al. (2015). The resulting large air velocities  
 317 may then be subsequently diffused back across the interface into the water, the degree

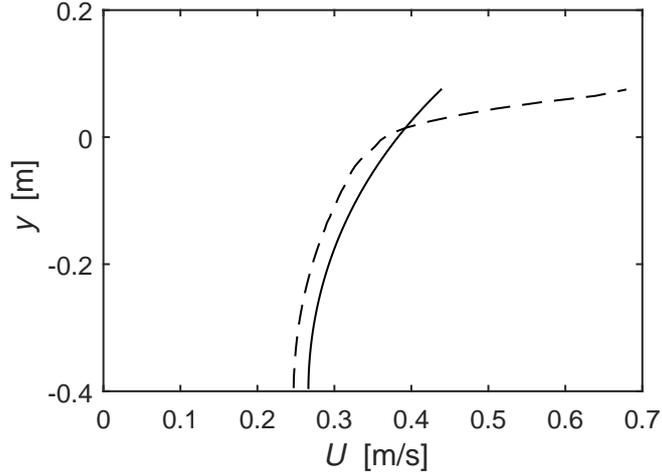


Figure 4. Simulated velocity distribution beneath the crest (- -) and stream function solution, (-) at  $t = 5T$ .

318 to which will be discussed in Section 4.4.

#### 319 4.2. Effect of the Courant number, $Co$

320 With the poor performance previously shown using the default `damBreak` settings,  
 321 two natural places to attempt improvement in the solution would be in the temporal  
 322 and spatial resolutions. In this section the effect of the temporal resolution will be  
 323 investigated by varying  $Co$ .

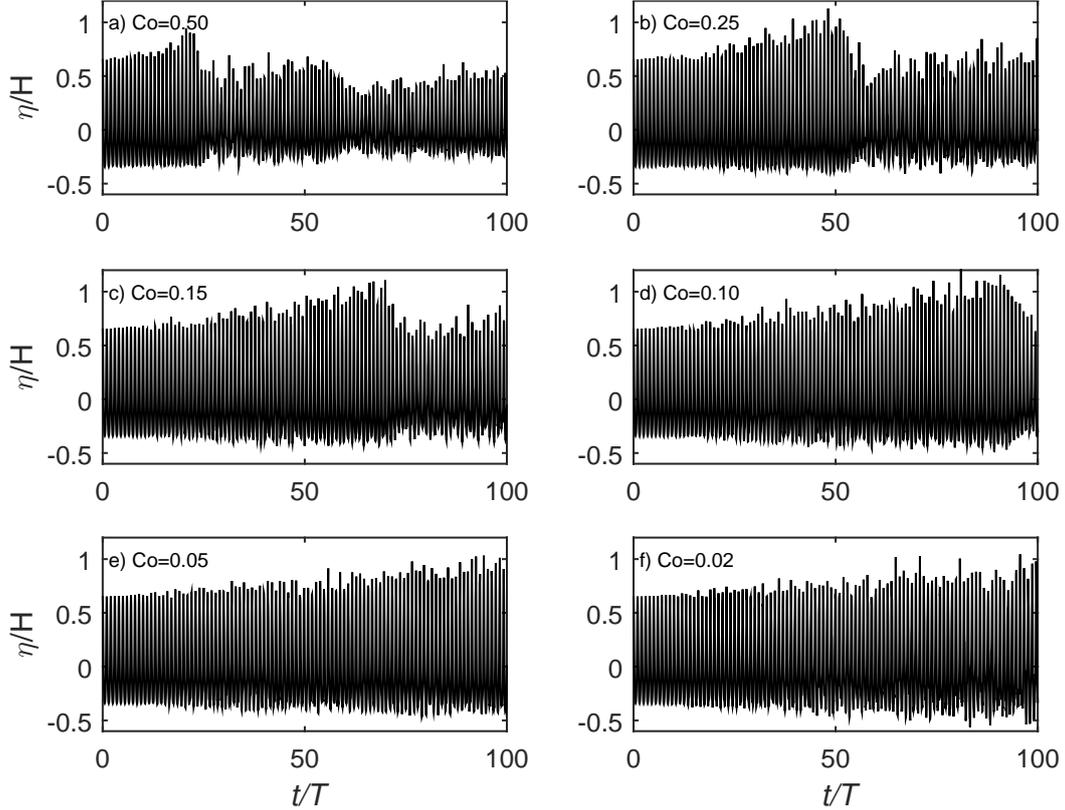
324 Figure 5 shows the surface elevation as a function of time for six different values of  
 325  $Co$ . From this it is evident that lowering  $Co$  has a significant impact on `interFoam`'s  
 326 performance. However, even with  $Co = 0.02$  `interFoam` is not capable of keeping the  
 327 wave shape for 100 periods as the wave heights are still seen to increase. Up until 20  
 328 wave periods the wave height is close to constant when using  $Co \leq 0.15$ . The wave is  
 329 still leading the analytical stream function solution and in general lowering  $Co$  reduces  
 330 the overestimation of the wave celerity as can be seen in table 2 where the phase-shift  
 331 at  $t = 25T$  is shown for the six different values of  $Co$ . The phase shift is calculated  
 332 as  $\phi_{shift} = (t_{peak} - t_{analytical})/T \cdot 360^\circ$ , where  $t_{peak}$  is the time where the crest of the  
 333 wave passes the sampling position, and  $t_{analytical}$  is the time where the stream function  
 solution should have passed the sampling position.

Table 2. Phase-shift at  $t = 25T$ .

$Co$	0.02	0.05	0.10	0.15	0.25	0.50
$\phi_{shift} [^\circ]$	0.0	0.0	-18	-36	-72	-198

334

335 Figure 6 shows the velocity profiles beneath the crest at  $t = 5T$  for the six different  
 336 values of  $Co$  together with the stream function solution, similar to Figure 4. It can  
 337 be seen that as  $Co$  is lowered the simulated velocity profiles become closer to the  
 338 analytical solution. The reason for this is probably two-fold. First, lowering  $Co$  delays  
 339 the presence and growth of the interface wiggles and thus also the steepening of the  
 340 wave. Second, any inconsistent treatment of the force balance near the free surface  
 341 is substantially limited by the small time step as it reduces e.g. the error committed  
 342 in linearising the convective term  $u_j(\partial\rho u_i/\partial x_j)$ . The importance of keeping a low  
 343 time step in `interFoam` when doing two-phase simulations has also been highlighted



**Figure 5.** Simulated surface elevation as a function of time for six different Courant numbers (Main fixed parameters:  $N = 12.5$ ,  $\text{ddt-Euler}$ ,  $\text{grad-Gauss Linear}$ ,  $\text{div}(\rho*\phi,U)\text{- Gauss LimitedLinearV 1}$ ,  $\text{laplacian-Gauss linear corrected}$ ,  $c_\alpha = 1$ ).

344 by Deshpande et al. (2012) in the context of surface tension dominated flows, where  
 345 it was shown that a small time step is crucial for limiting the growth of spurious  
 346 velocities. Even though the present inertia dominated situation is different from the  
 347 analysis of Deshpande et al. (2012), the solution to minimize the interface imbalance  
 348 by limiting the time step still seems to hold.

349 In addition to the velocity profiles depicted in Figure 6, it is also of interest to see  
 350 how the overestimation of the crest velocity evolves in time. Therefore, in Figure 7 the  
 351 error in the crest velocity calculated as

$$\Delta E = \frac{\max(U) - U_{\text{analytical}}}{U_{\text{analytical}}} \quad (12)$$

352 is shown for each of the six values of  $Co$  considered. Regardless of  $Co$ , the overes-  
 353 timation of the crest velocity is apparent and grows in time. From Figure 7 it can  
 354 be seen that even with a relatively small  $Co$ , e.g.  $Co = 0.15$ , after only propagating  
 355 five periods, the crest velocity is approximately 17% larger than the analytical. It thus  
 356 seems that, what is generally viewed as a rather "low"  $Co$ , is still not sufficiently small  
 357 to accurately simulate surface waves. In contrast, the error in the crest velocity for  
 358 the case with  $Co = 0.05$  is only 0.1% after five periods, thus this value seems like a  
 359 proper  $Co$  for the accurate simulation of this wave. These results indicate that many  
 360 previous simulations of free-surface waves have not achieved time step convergence.

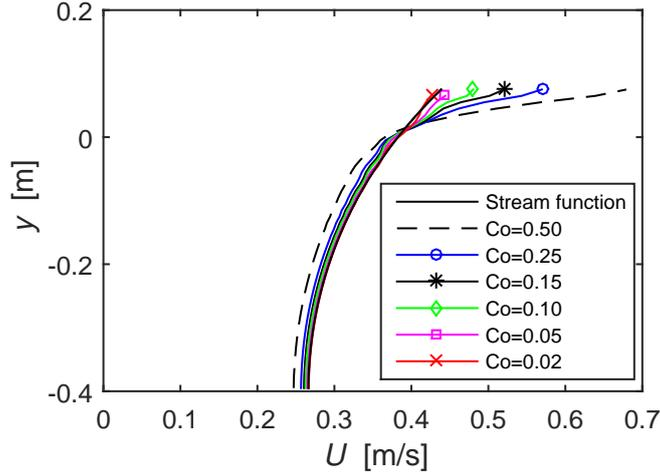


**Figure 6.** Velocity distribution beneath the crest at  $t = 5T$  for various Courant numbers (Main fixed parameters:  $N = 12.5$ , `ddt-Euler`, `grad-Gauss Linear`, `div(rho*phi,U)-Gauss LimitedLinearV 1`, `laplacian-Gauss linear corrected`  $c_\alpha = 1$ ).

### 361 4.3. The effect of mesh resolution

362 Having checked the effect of the temporal resolution, it now seems natural to check the  
 363 effect of varying the spatial resolution. However, as the solution with  $Co = 0.5$  from the  
 364 `damBreak` tutorial was poor, the rest of the forthcoming analysis will be continued with  
 365  $Co = 0.15$ , with the hope of further improving the previous results. In Jacobsen et al.  
 366 (2012) it was noted that `interFoam` performed best with cell aspect ratios, defined  
 367 as  $\Delta x/\Delta y$ , of 1, and this ratio will be maintained throughout the analysis. In the  
 368 previous cases  $N = 12.5$ , and now three additional simulations will be performed with  
 369  $N = 50$ ,  $N = 25$  and  $N = 6.25$  respectively. Figure 8 shows the surface elevations as  
 370 a function of time for the four different resolutions. Similar to increasing the temporal  
 371 resolution (i.e. lowering  $Co$ ) it can be seen that increasing the number of cells per  
 372 wave height greatly improves the solution when considering the ability to propagate the  
 373 wave while maintaining constant form.

374 Before continuing, it is also worth commenting on the shape of the air–water inter-  
 375 face in the different resolutions, which is illustrated in Figure 9 for  $N = 6.25$  and  
 376  $N = 25$ . As expected with  $N = 6.25$  the interface looks smeared and is not well cap-  
 377 tured. With  $N = 12.5$  (not shown here for brevity) the interface looks similar to Figure  
 378 2a, but the wave gradually steepens in time as previously explained. With  $N = 25$   
 379 and also  $N = 50$  the interface is even sharper and with  $N = 25$  the wave heights were  
 380 also seen to increase, but somewhat slower. This is probably related to the size of the  
 381 wiggles being much smaller with the finer mesh. In these cases the wiggles were not  
 382 only present in the top of the crest, but also along the whole wave surface. They also  
 383 appeared at an earlier time, as seen in Figure 9b.

384 In Figure 10 the velocity profiles beneath the crest at  $t = 5T$  are shown for the four  
 385 different spatial resolutions together with the analytical stream function solution. In  
 386 general, it can be seen that, improving the spatial resolution improves the solution.  
 387 However, for the case with  $N = 25$  the crest velocity is as high as in the coarser resolved  
 388 cases. This can be explained by the afore mentioned wiggles. At the crest of such a  
 389 surface wiggle, the velocity is much higher compared to the rest of the wave. This is  
 390 not seen to the same degree with  $N = 50$  where the surface wiggles are much smaller.  
 391 When propagating the wave longer than the five periods, it was experienced that the

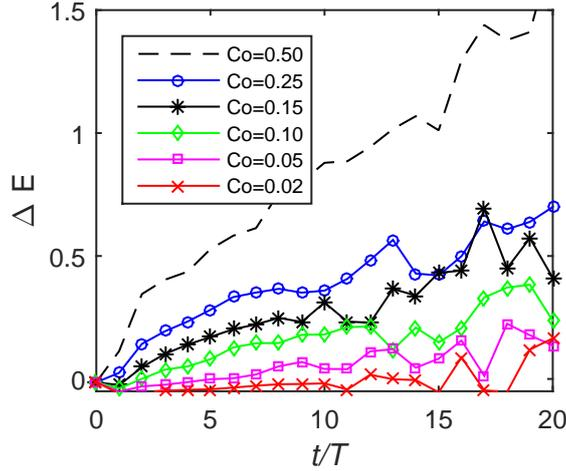


**Figure 7.** Error in the maximum crest velocity as a function of periods (Main fixed parameters:  $N = 12.5$ , ddt-Euler, grad-Gauss Linear, div(rho\*phi,U)-Gauss LimitedLinearV 1, laplacian-Gauss linear corrected  $c_\alpha = 1$ ).

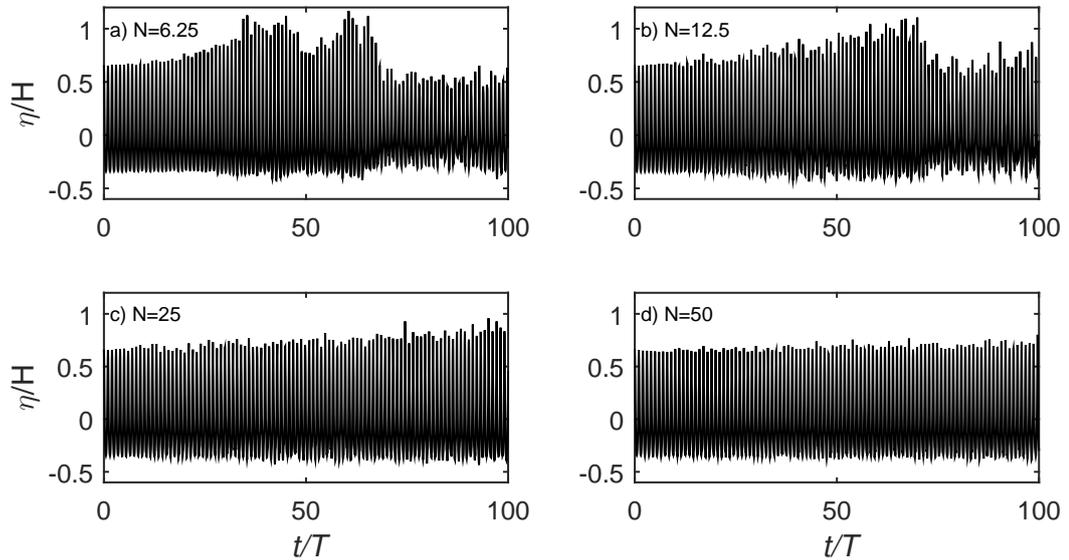


**Figure 8.** Simulated surface elevation as a function of time for four different mesh resolutions (Main fixed parameters:  $Co = 0.15$ , ddt-Euler, grad-Gauss Linear, div(rho\*phi,U)-Gauss LimitedLinearV 1, laplacian-Gauss linear corrected  $c_\alpha = 1$ ).

392 case with  $N = 25$  had crest velocities closer to the analytical solution than the two  
 393 coarser resolved cases. From the above results it is worth noting that increasing the  
 394 spatial resolution was not able to produce as good results for the velocity profiles as  
 395 increasing the temporal resolution, see Figures 6 and 10. From a computational point  
 396 of view decreasing  $Co$  seem to be a more efficient alternative to increase accuracy, than  
 397 increasing the mesh resolution. This is especially true considering that increasing the  
 398 mesh resolution, will also make the time step decrease to maintain a given  $Co$ . However,  
 399 in terms of keeping the wave height constant for the entire simulation, increasing the  
 400 spatial resolution does seem to yield better results compared to simply increasing the  
 401 temporal resolution.

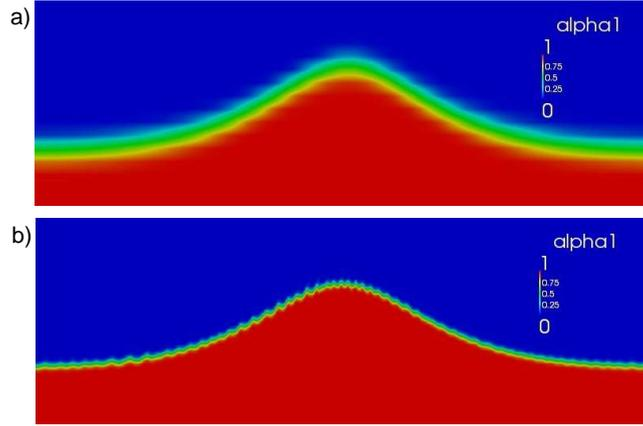


**Figure 9.** Snapshot at  $t = 5.5T$  for a)  $N = 6.25$  and b)  $N = 25$  (Main fixed parameters:  $Co = 0.15$ , ddt-Euler, grad-Gauss Linear, div(rho\*phi,U)-Gauss LimitedLinearV 1, laplacian-Gauss linear corrected  $c_\alpha = 1$ ).

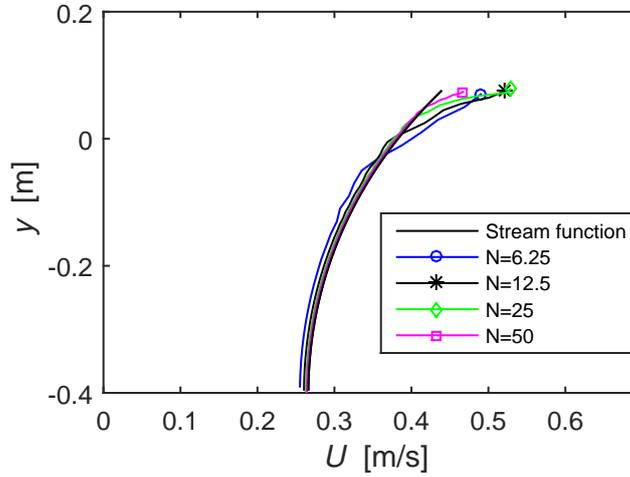


**Figure 10.** Velocity distribution beneath the crest at  $t = 5T$  for various mesh resolutions (Main fixed parameters:  $Co = 0.15$ , ddt-Euler, grad-Gauss Linear, div(rho\*phi,U)-Gauss LimitedLinearV 1, laplacian-Gauss linear corrected  $c_\alpha = 1$ ).

#### 402 4.4. *fvSchemes and fvSolution settings*

403 Thus far increasing the temporal and spatial resolution have been attempted, and  
 404 unsurprisingly, these improved the solution. For the rest of this study  $Co = 0.15$   
 405 and  $N = 12.5$  will be maintained for the sake of balancing computational costs and  
 406 accuracy, and the additional effects of changing schemes and solution settings will be  
 407 investigated. As quite a few schemes are available, not all results of our investigations  
 408 will be shown. Our findings will be summarized and figures will be included when  
 409 found to be most relevant. Later, we will combine some of the investigated schemes to  
 410 improve the overall solution quality.

411 It has been shown that the interface between air and water in time develop wiggles,  
 412 which in time grow and sometimes lead to breaking. First, the additional effects of  
 413 modifying `cAlpha` (with default value  $c_\alpha = 1$ ), which controls the size of the compression  
 414 velocity, will be investigated. It was experienced that increasing  $c_\alpha$  causes the  
 415 wiggles to appear earlier and grow faster. Reducing  $c_\alpha$  reduces the wiggles and at the

416 same time causes the interface to smear out over more cells. This strongly indicates  
 417 that the wiggles are caused by the numerical interface compression method.

418 To illustrate the effect of  $c_\alpha$ , the surface elevations are shown for four different values  
 419 in Figure 11. In this figure, to demonstrate the effect of  $c_\alpha$  on the interface, we also  
 420 plot the  $\alpha = 0.99$  and  $\alpha = 0.01$  contours for the crest and the trough for each period.  
 The reduction in wave height seen in the case with  $c_\alpha=0$  (Figure 11a), is the effect

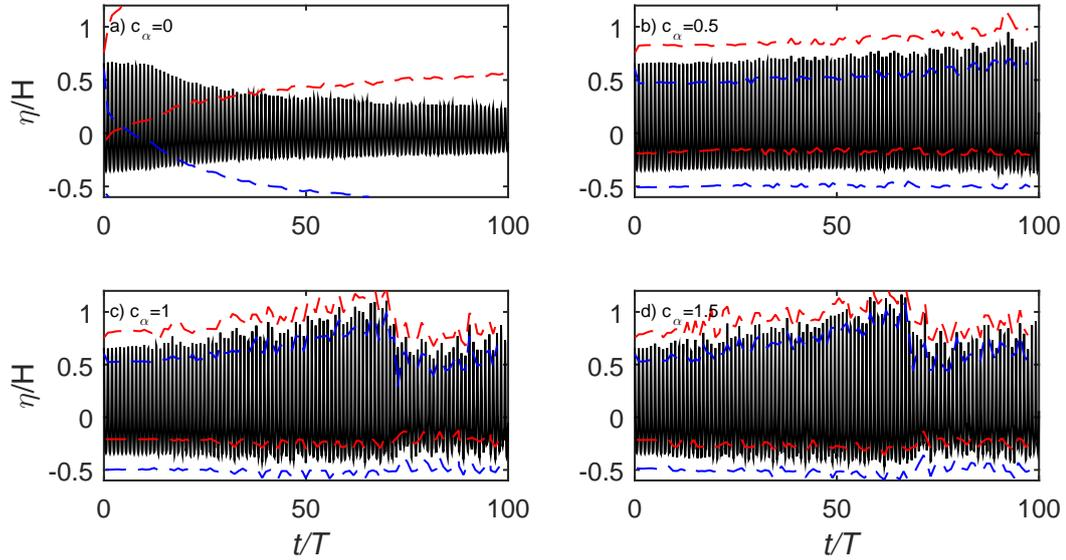


**Figure 11.** Simulated surface elevations (-) as a function of time for different values of  $c_\alpha$  together with the  $\alpha = 0.99$  and  $\alpha = 0.01$  contours (- -) (Main fixed parameters:  $Co = 0.15$ ,  $N = 12.5$ , ddt-Euler, grad-Gauss Linear, div(rho\*phi,U)-Gauss LimitedLinearV 1, laplacian-Gauss linear corrected).

421 of a very heavy diffusion of the interface. This can be seen even more clearly when  
 422 looking at the  $\alpha = 0.99$  and  $\alpha = 0.01$  contours. It can be seen that after 20 periods  
 423 the 0.99 contour at the crest is actually positioned lower than the trough level and  
 424 the 0.01 contour at the trough is almost at the crest level. The distance between the  
 425 0.01 contour and 0.99 contour is approximately four cells with  $c_\alpha = 0.5$  (Figure 11b),  
 426 whereas it only spans approximately three cells for  $c_\alpha = 1$  (Figure 11c) and  $c_\alpha = 1.5$   
 427 (Figure 11d). This shows that increasing  $c_\alpha$  does compress the interface, but that the  
 428 interface will span more than one cell, even with a high value of  $c_\alpha$ .  
 429

430 In addition to the  $c_\alpha$  value, various other settings affect the size and behaviour of  
 431 the wiggles, and in the following  $c_\alpha = 1$  will be maintained, for the sake of comparison.  
 432 The effect of the time discretization scheme on the surface elevations is shown in Figure  
 433 12. Changing the time discretization scheme from **Euler** (first order) to **CN** (second  
 434 order) exacerbates the wiggle feature, causing them to develop earlier and extend  
 435 throughout the surface. Contrary to results utilizing the **Euler** scheme, the wiggles  
 436 do not cause the wave to steepen to the same extent. The wiggles grow in size, but  
 437 they often break on top of the wave before merging, and therefore the wave does not  
 438 steepen as much as with the **Euler** scheme. It is believed that the wiggle feature is  
 439 more pronounced with the **CN** scheme simply because the scheme is less diffusive than  
 440 the **Euler** scheme. The artificial compression term, as just shown, adds some erratic  
 441 behaviour to the interface, and this is diffused by numerical damping when using the  
 442 **Euler** scheme, but less so when using **CN**.

443 The reduction or complete removal of wiggle formations is also seen utilizing other

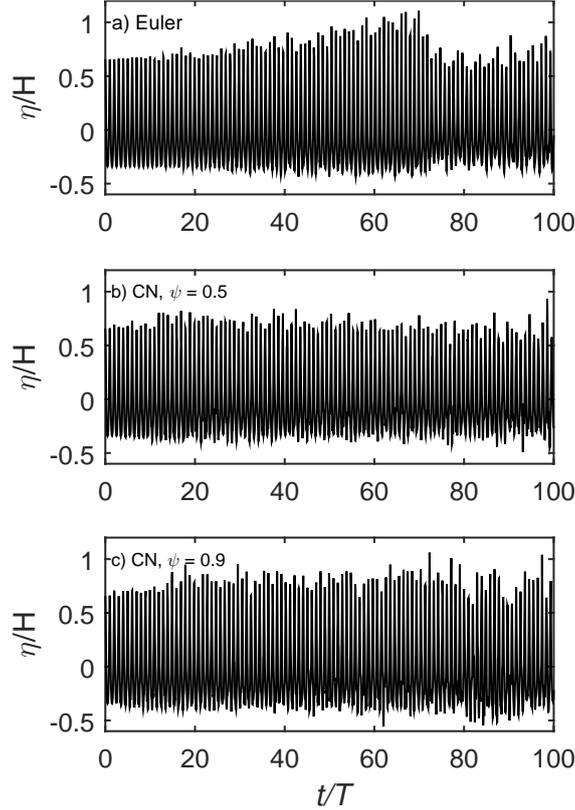


**Figure 12.** Simulated surface elevation as a function of time for different time discretization schemes (Main fixed parameters:  $Co = 0.15$ ,  $N = 12.5$ , `grad-Gauss Linear`, `div(rho*phi,U)-Gauss LimitedLinearV 1`, `laplacian-Gauss linear corrected`,  $c_\alpha = 1$ ).

444 more diffusive schemes, e.g. when using the upwind scheme for the convection of the  
 445  $\alpha$  field or using the upwind scheme for the convection of momentum. In the case of  
 446 utilizing the upwind scheme for the convection of the  $\alpha$  field the solution is very similar  
 447 to that seen when setting  $c_\alpha = 0$  (Figure 11a), with the interface experiencing heavy  
 448 diffusion and the resulting wave height decaying rapidly. Utilizing an upwind scheme  
 449 for the convection of momentum also causes the wave height to decay, but at a much  
 450 slower rate, and is not accompanied by the same degree of interface diffusion. However,  
 451 utilizing a pure upwind scheme is generally not recommended due to excessive smearing  
 452 of the solution.

453 Thus far it has been shown that  $c_\alpha$  and the time discretization scheme have a sig-  
 454 nificant impact on the surface elevation and interface. However, regarding the velocity  
 455 profile beneath the crest (not shown here for brevity), the impact is very small, except  
 456 for the case with  $c_\alpha = 0$ , which made made the velocities throughout the water column  
 457 beneath the crest too low. This is probably due to heavy diffusion of the interface (see  
 458 Figure 11a).

459 As mentioned, the wiggles can be limited by choosing more diffusive schemes, but  
 460 it still needs to be determined how these schemes affect the general propagation of  
 461 the wave and the underlying velocity profile. Figure 13 shows the surface elevation for  
 462 four different convection schemes (`div(rho*phi,U)`), and the influence of the choice  
 463 on convection scheme is readily apparent. The most diffusive among the four schemes,  
 464 the `upwind` scheme, makes the wave decay in a quite stable fashion (Figure 13b).

465 The SFCD scheme (Figure 13c) is slightly more diffusive than the `limitedLinearV 1`  
 466 scheme (Figure 13a), and is seen to limit the growth in the wave height. The wave  
 467 height still increases as time progresses but the increase is delayed and the simulation  
 468 is less erratic. The fourth scheme is the `SuperBee` scheme (Figure 13d). This scheme  
 469 is also within the TVD family, but it is much more erratic, and almost immediately  
 the wave heights start to increase.

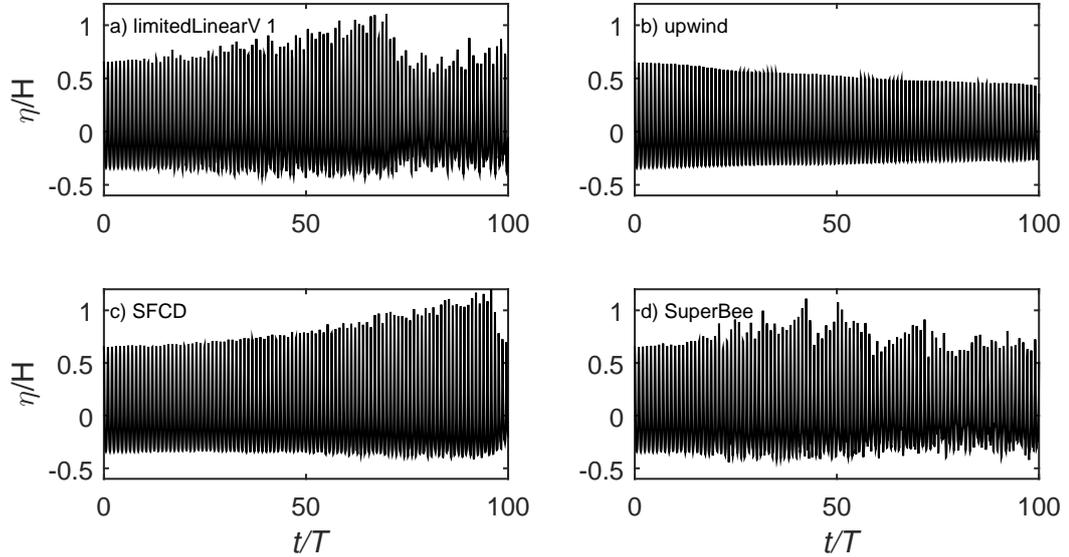


**Figure 13.** Simulated surface elevation as a function of time for different convection schemes (Main fixed parameters:  $Co = 0.15$ ,  $N = 12.5$ , `ddt-Euler`, `grad-Gauss Linear`, `laplacian-Gauss linear corrected`,  $c_\alpha = 1$ ).

470

471 The velocity profiles beneath the crest for the four convection schemes are like-  
 472 wise shown at  $t = 5T$  in Figure 14, and once again the importance of the convection  
 473 scheme is quite clear. The `upwind` scheme limits the error in the velocity at the top  
 474 crest whereas it underestimates the velocity closer to the bed. The SFCD scheme be-  
 475 haves slightly better than the `limitedLinearV 1` scheme, and the `SuperBee` scheme  
 476 performs the worst. When propagating further the `SuperBee` scheme has oscillations  
 477 in the velocity profile beneath the crest, which can also be seen to a smaller degree in  
 478 Figure 14.

479

480 A range of other convection schemes have also been attempted. None of them,  
 481 however, show significantly different results than those shown here, which have been  
 482 selected to demonstrate the effect of convection scheme diffusivity on the propagation  
 483 of the wave and velocity profile beneath the crest. While the convection schemes have  
 484 been shown to have a great effect on both the ability to maintain a constant wave  
 485 height, limit the wiggle feature in the interface and predict the velocity profile, it is  
 486 not directly evident which scheme performs the best overall. The `upwind` scheme limits  
 487 the error in the crest velocity the most, which would be beneficial when e.g. doing loads  
 488 e.g. vortex shedding around such a structure. The SFCD scheme improves the ability to  
 489 maintain a constant wave height and limits the growth in the crest velocity compared  
 490 to the `limitedLinearV 1` scheme from the `damBreak` tutorial, but the crest velocity  
 491 is still severely overestimated.

492

493 We will now turn our attention to the gradient (`grad`) schemes. These effects (rela-  
 tive to the default `Gauss Linear` scheme in Figures 5c and 6) on the wave propa-

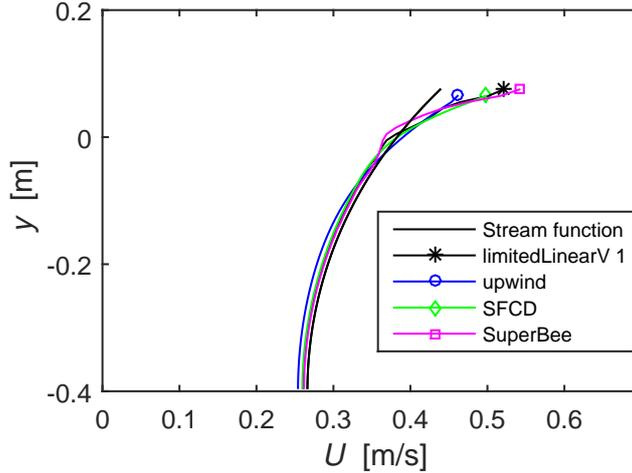


**Figure 14.** Velocity distribution beneath the crest at  $t = 5T$  for various convection schemes (Main fixed parameters:  $Co = 0.15$ ,  $N = 12.5$ , `ddt-Euler`, `grad-Gauss Linear`, `laplacian-Gauss linear corrected`,  $c_\alpha = 1$ ).

494 gation and velocity profile will be described, but for brevity no additional figures will  
 495 be included. The fourth-order scheme (`fourth`) improves the propagation and delays  
 496 the increase in wave heights, similar to the behaviour seen with the `SFCD` convective  
 497 scheme (Figure 13c), which is more diffusive than the standard `limitedLinearV 1`  
 498 scheme. The `fourth` scheme is however not more diffusive than the `Gauss Linear`  
 499 scheme, and the delayed increase in wave height is probably due to the scheme  
 500 having higher-order accuracy. The velocity profile beneath the crest, on the other  
 501 hand, is not improved relative to the `Gauss Linear` scheme (Figure 6,  $Co=0.15$ ). The  
 502 `faceMDLimited Gauss Linear 1` gradient scheme has also been tested, and behaves  
 503 very similar to the `upwind` convection scheme (Figure 13b), in the sense that the wave  
 504 heights decrease with time. The reason for this is probably that the gradient limiter,  
 505 coupled with the `limitedLinearV 1` convection scheme, effectively makes the con-  
 506 vection scheme an upwind scheme. With respect to the velocities the `faceMDLimited`  
 507 gradient scheme produced a velocity profile very similar to that from the `upwind`  
 508 scheme (Figure 14). That the limited gradient scheme can produce results similar to  
 509 the `upwind` convection scheme was also observed by Liu and Hinrichsen (2014), who  
 510 studied the effect of convection and gradient schemes on bubbling fluidized beds using  
 511 `OpenFOAM`.

512 We will now describe how changing the Laplacian scheme effects the solution, rela-  
 513 tive to the default setting (`Gauss linear corrected`). As previously mentioned the  
 514 Laplacian scheme requires keywords for both `interpolation` and `snGrad`, but the in-  
 515 puts for the stand alone `interpolation` and `snGrad` schemes are not changed. For the  
 516 Laplacian scheme, combining the `Gauss linear` interpolation with the `fourth snGrad`  
 517 scheme, resulting in the Laplacian scheme `Gauss Linear fourth`, gave improved re-  
 518 sults, both in terms of the ability to maintain constant wave heights and in terms of  
 519 the velocity profile beneath the crest. However switching to the fourth-order scheme  
 520 (`fourth`), resulted in very high spurious velocities in the air region above the wave,  
 521 and hence (due to the  $Co$ -controlled time step) leads to reductions in the time steps  
 522 used during the simulation. In this way changing to a fourth-order `snGrad` schemes in  
 523 the Laplacian is effectively similar to lowering  $Co$ . To check whether the fourth-order  
 524 `snGrad` scheme in the Laplacian really improved the solution, or if it is merely a result

525 of a reduced time step, two additional simulations, now utilizing a fixed time step  
 526  $dt=0.0025$  s, have been performed, with both `corrected` and `fourth snGrad` scheme  
 527 in the Laplacian. The resulting velocity profiles at  $t = 5T$ , together with the result  
 528 from a simulation with  $\rho_{air} = 0.1$  kg/m<sup>3</sup> (also utilizing the same fixed time step), are  
 shown in Figure 15. The three simulations show similar results in the water phase,

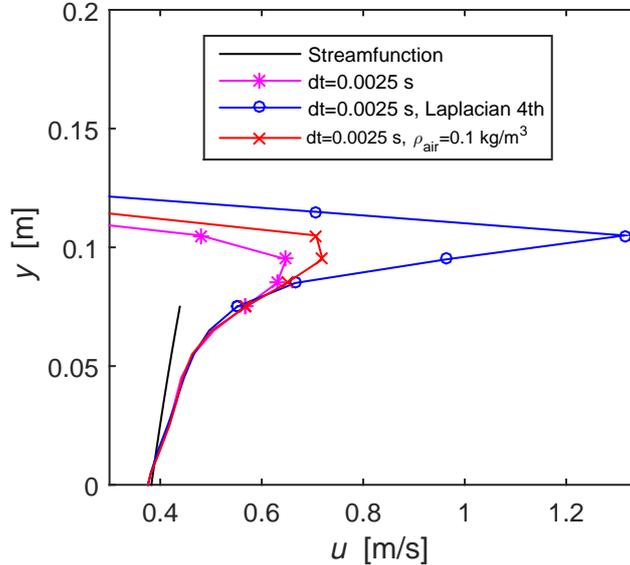


**Figure 15.** Velocity distribution beneath the crest at  $t = 5t$  with a fixed time step utilizing the standard setup as well as 4th order Laplacian and  $\rho_{air} = 0.1$  kg/m<sup>3</sup>. Full lines represent the velocities in pure water and the lines with symbols represent the velocities in the air or mixture cells (Main fixed parameters:  $N = 12.5$ , `ddt-Euler`, `grad-Gauss Linear`, `div(rho*phi,U)-Gauss LimitedLinearV 1`,  $c_\alpha = 1$ )

529 but rather different velocities in the air phase. These results indicate that, while being  
 530 an un-physical and undesirable phenomenon, the spurious velocities in the air do not  
 531 seem to effect the wave significantly. The case with a fourth-order `snGrad` scheme had  
 532 approximately twice as high air velocities as the standard set up, but similar (actu-  
 533 ally slightly lower) crest velocities. The case with lower density also has higher air  
 534 velocities, but very similar water velocities to the standard case. To summarize: Even  
 535 though the fourth-order Laplacian scheme is able to produce better wave kinematics,  
 536 caution must be taken as it produces large spurious velocities. These will, utilizing a  
 537 variable time step, lead to very low time steps. Alternatively, a fixed time step may  
 538 result in an unstable Courant number.

540 Before conducting the present study it was expected that the discretization schemes  
 541 would have an effect on the solution, but it was also expected that in particular the  
 542 choice of iterative solvers for the pressure would not have an effect, at least if the tol-  
 543 erances were sufficiently low. It turns out, however, that the iterative solver settings  
 544 in `fvSolution` also affect the wave propagation. For the pressure equations (`pcorr`,  
 545 `pd` and `pdFinal`) switching from `PCG` to `GAMG` made the simulations more erratic as  
 546 the wave broke much earlier (however the simulation time was much lower), whereas  
 547 switching to a smooth solver (`smoothSolver`) did not affect the quality of the solution,  
 548 but took much longer time. It was also attempted to lower the tolerance by a factor  
 549 1000 on both the pressure and the velocity, but hardly any difference in the solution  
 550 was seen. For the controls of the solution algorithm increasing the number of alpha cor-  
 551 rectors, `nAlphaCorr`, as well as alpha subcycles, `nAlphaSubCycles`, improved, though  
 552 not dramatically, the propagation of the wave in terms of it maintaining its' shape,

553 whereas increasing the number of correctors, `nCorrectors` did not change anything.  
554 Increasing the number of outer correctors, `nOuterCorrectors` (`nOCorr`), effectively  
555 making it into the PIMPLE algorithm, surprisingly made the wave height decrease  
556 very rapidly. This behaviour was also seen in Weber (2016) and will be investigated  
557 further in the forthcoming section.

558 The choice of iterative solvers could also potentially effect the velocity profile. The  
559 `GAMG` solver produced much higher crest velocities (close to that seen with  $Co = 0.5$  in  
560 Figure 4). The `SmoothSolver`, which was a lot slower, produced an almost identical  
561 velocity profile to the `PCG` solver (Figure 6,  $Co = 0.15$ ). Lowering the tolerances by a  
562 factor 1000 had almost no effect on the surface elevation, and the effect on the velocity  
563 profile was also negligible. Changing the number of  $\alpha$  subcycles (`nAlphaSubCycles`),  
564  $\alpha$  correctors (`nAlphaCorr`) and number of correctors (`nCorrectors`) did not influence  
565 the crest velocity in any significant way, and raising the number of  $\alpha$  correctors actually  
566 worsened the result closer to the bed.

567 It has now been shown that the discretization schemes and solution procedures have  
568 a potentially large impact in the solution, both in terms of the wave height and velocity  
569 profile, as well as the wiggles in the interface and the spurious air velocities. Using more  
570 diffusive schemes than the base setup from the `damBreak` tutorial has been shown to  
571 limit or remove the growth of the wiggles, limit the overestimation of the crest velocity,  
572 and also limit the growth of the wave heights. However, the more diffusive schemes  
573 were seen to smear the interface, and could potentially be more inaccurate for other  
574 situations. The demonstration of the large importance of the discretization schemes  
575 on the accuracy of the solution can be considered an important finding in its own as  
576 this has not previously been documented but only hinted e.g. by Paulsen et al. (2014);  
577 Wroniszewski et al. (2014).

#### 578 4.5. *Combined schemes*

579 It would be ideal to achieve a setup capable of propagating a wave for 100 periods,  
580 while keeping a relatively large time step and at the same time maintaining both its  
581 shape and the correct velocities. Changing one single scheme has not achieved that. It  
582 was however shown that adding some diffusion in some of the schemes could mitigate  
583 both the increase in wave height as well as the increased near-crest velocities.

584 To test whether a combination of schemes can improve the solution further, the  
585 `upwind` scheme on the convection of momentum, which was actually seen to cause  
586 the wave to decay (Figure 13b), will be combined with the slightly less diffusive  
587 blended CN scheme (Figure 12c). It is also attempted to increase the artificial compression,  
588 by increasing  $c_\alpha$  while picking a more diffusive scheme for the gradient, namely  
589 `faceMDLimited` which also caused the wave height to decrease. Finally, the outer correctors  
590 are increased to two and combined with the blended CN scheme, together with  
591 the `SFCD` scheme for the momentum flux.

592 The surface elevations for three such combinations are seen in Figure 16b–d. Here  
593 it can be seen that by combining the diffusive `upwind` scheme for the convection of  
594 momentum and shifting from the more diffusive `Euler` scheme to a less diffusive CN  
595 scheme (Figure 16b) can maintain the wave height for the entire 100 periods. The  
596 same can be done by increasing the compression factor  $c_\alpha$  while maintaining a more  
597 diffusive gradient scheme (Figure 16c, although in this case the wave heights actually  
598 decayed a bit), and also by increasing the number of outer correctors together with  
599 the CN scheme (Figure 16d). The latter results in slightly more variations in the wave

600 height, but also utilized a much higher blending value in the CN scheme, which can  
 601 cause oscillations in the solution and, as previously shown, excite wiggles in the free  
 602 surface. All three cases show a great improvement compared to the original default  
 case, repeated as Figure 16a to ease comparison. It should also be stated that the

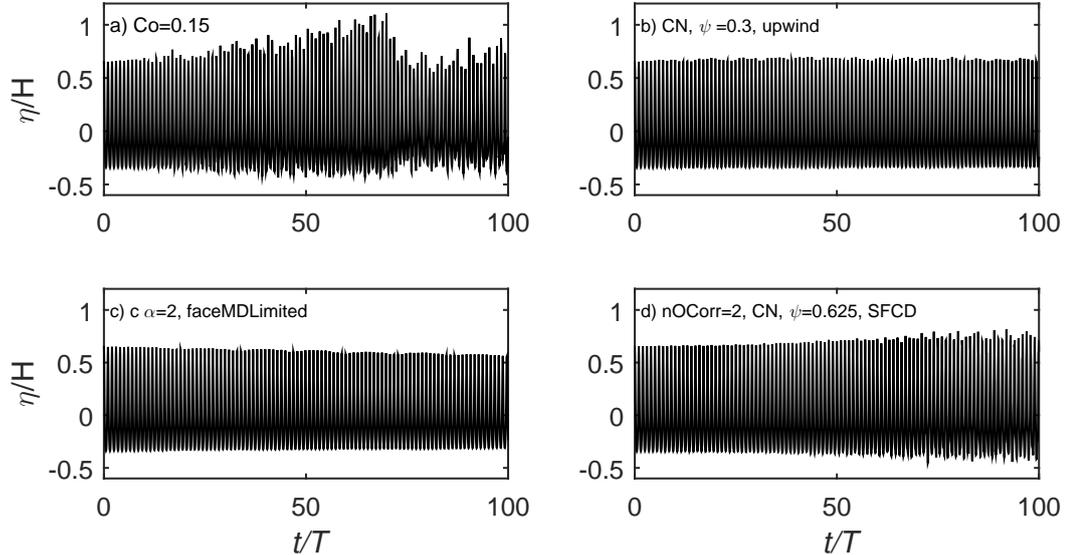


**Figure 16.** Simulated surface elevation as a function of time for different schemes (Main fixed parameters:  $Co = 0.15$ ,  $N = 12.5$ , `laplacian-Gauss linear corrected`).

603  
 604 balance obtained for the case with the outer correctors is particularly delicate. First  
 605 it was attempted to run with two outer correctors and a blended CN scheme, while  
 606 maintaining the `limitedLinearV 1` scheme on the momentum flux. This however  
 607 caused wiggles in the interface, as also previously described, and therefore the `SFCD`  
 608 scheme was chosen to counteract the wiggles. The wiggles were not removed altogether  
 609 with the `SFCD` scheme, but their presence was significantly delayed. Further, the best  
 610 result was obtained with CN,  $\psi = 0.625$ , but lowering the blending factor to  $\psi = 0.6$   
 611 made the wave height decrease slightly over the 100 periods, and raising it to  $\psi = 0.65$   
 612 made it increase slightly and caused more wiggles.

613 The resulting velocity profiles beneath the crest at  $t = 5T$  for the three cases shown  
 614 in Figure 16b-d are shown in Figure 17, together with the velocity profile obtained  
 615 utilizing the base settings. Here it is evident that all three combinations give lower  
 616 velocities in the crest than the standard setting. However the standard setup shows  
 617 a slightly better comparison with the analytical result closer to the bottom than the  
 618 case utilizing `upwind` for the momentum flux together with CN as well as the case  
 619 utilizing  $c_\alpha = 2$  together with the `faceMDLimited` gradient scheme. The final combi-  
 620 nation, utilizing two outer correctors together with a blended CN scheme and a `SFCD`  
 621 scheme shows a significantly better result, and is very similar to the analytical profile.  
 622 It can be seen that there are small odd oscillations in the profile of this case, and  
 623 these oscillations actually become larger as the wave propagates. Nevertheless, this  
 624 significant improvement is achieved with minimal increase in computational expense,  
 625 especially compared to the results obtained utilizing the settings from the `damBreak`  
 626 tutorial. The improvement in the velocity profile with the outer correctors is inter-  
 627 preted as the outer correctors ensuring a better coupling between velocity, pressure  
 628 and the free-surface.

629 It has now been shown that it is possible to achieve a "diffusive balance" in the

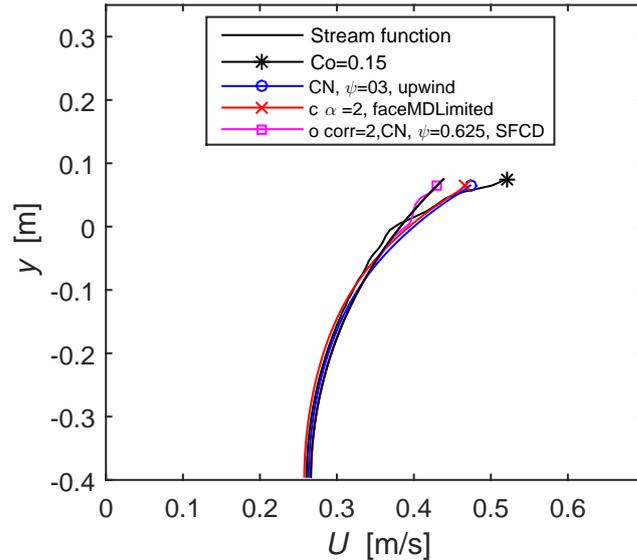


**Figure 17.** Velocity distribution beneath the crest at  $t = 5T$  for various combined schemes (Main fixed parameters:  $Co = 0.15$ ,  $N = 12.5$ , `laplacian-Gauss linear corrected`).

630 schemes, that enables `interFoam` to progress the wave while maintaining its shape.  
631 The same diffusive balance is also shown to limit, but (except for the case utilizing  
632 outer correctors) not eliminate, the overestimation of the velocity in the crest. This  
633 diffusive balance is, however, not universal. What seems a proper amount of diffusion  
634 in the case of  $Co = 0.15$  is not so with a lower  $Co$  where the error in velocity of the crest  
635 is much smaller, and more diffusive schemes would actually worsen the solution. Also,  
636 what gives the best balance for this wave, might not give the best balance for a wave  
637 with another shape, but the present study reveals a generic strategy that can be fine  
638 tuned for individual cases. Interestingly, this implies that for variable depth problems,  
639 where waves would not maintain a constant form, there may not be a globally optimal  
640 combination. Nevertheless, it is still hoped that better-than-default accuracy can be  
641 achieved with the combinations suggested herein.

#### 642 4.6. Summary of experience using `interFoam`

643 To summarize our experience using `interFoam` from this section: The safest way to  
644 get a good and stable solution is by using a small Courant number. If the time step  
645 is low enough, `interFoam` is capable of producing quite good results. However, due  
646 to limited time or computational resources, this solution may often not be realistic in  
647 practice.

648 If wishing to use larger time steps, alternatively, it is advised to try to obtain a  
649 diffusive balance. The best choice can then be determined on a case by case basis,  
650 though it is hoped that the examples utilized above may be a good starting point for  
651 more general situations. If looking to simulate e.g. wave breaking, the incoming waves  
652 could first be simulated in a cyclic domain, as done herein, prior to doing the actual  
653 larger-scale simulation. In this smaller simulation, the proper balance between, diffu-  
654 sivity, time step, computational expense and solution accuracy could be determined,  
655 before doing more advanced simulations. This should help ensure that reasonable ac-  
656 curacy in the initial propagation is maintained, which is important as this will affect

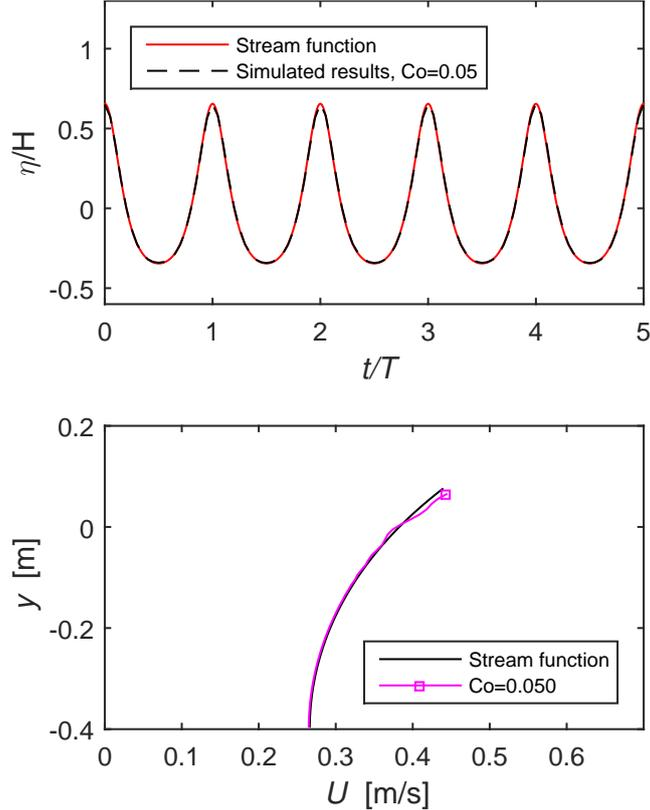


**Figure 18.** Surface elevations and velocity distribution beneath the crest at  $t = 5T$  for  $Co = 0.05$  (Main fixed parameters:  $N = 12.5$ , `ddt-Euler`, `grad-Gauss Linear`, `div(rho*phi,U)-Gauss LimitedLinearV 1`, `laplacian-Gauss linear corrected`,  $c_\alpha = 1$ ).

657 the initial breaking point and hence the subsequent surf zone processes.

658 The present results have focused on a rather demanding task of simulating long-  
659 time CFD wave propagation over 100 periods, though the problem with the overes-  
660 timation of crest velocities show up much earlier (see again Figure 4). To underline  
661 that `interFoam` is capable of producing a good result for most practical applications  
662 involving shorter propagation horizons, without having to resort to a diffusive balance  
663 strategy, Figure 18 shows the surface elevations for the first five periods, as well as  
664 the velocity profile beneath the crest at  $t = 5T$  using a small  $Co = 0.05$ . Here a good  
665 match with the analytical stream function solution is achieved. A similar improve-  
666 ment in the prediction of the crest velocities, with reduction of Courant number, were  
667 shown in Roenby et al. (2017), and this thus seems to be a robust and generally viable  
668 strategy.

## 669 5. `interFoam` coupled with `isoAdvector`: `interFlow`

670 One of the problems with `interFoam` is that the surface gets smeared over several  
671 cells, as demonstrated in Section 4.4. This is mitigated by the artificial compression  
672 term, which makes the surface sharper, but (as shown herein, Figure 11) also produces  
673 some undesired effects. In this section we will finally test the results using `interFoam`  
674 coupled with the `isoAdvector` algorithm, recently developed by Roenby et al. (2016),  
675 which is also available in the newest version of `OpenFOAM` (`OpenFOAM-v1706`). The

676 `isoAdvect` version in `OpenFOAM-v1706` has a slightly different implementation of  
677 the outer correctors than the version used in the present study, see Roenby et al.  
678 (2017) for details. With `isoAdvect` the equation for  $\alpha$  (6) is not solved directly.  
679 Instead the surface is identified by an iso-line, similar to those shown for  $\alpha = 0.99$   
680 and  $\alpha = 0.01$  in Figure 11. After identifying the exact position of the surface, it  
681 is then advected in a geometric manner. For more details on the implementation of  
682 `isoAdvect` the reader is referred to Roenby et al. (2016).

683 The new `isoAdvect` algorithm, coupled with `interFoam` will for the remainder  
684 of this study be named `interFlow`. As a first case, `interFlow` and `interFoam` will be  
685 compared for the previously well-tested case with the `damBreak` settings and  $Co =$   
686  $0.15$ . It should be stated however, that `interFlow` was not able to propagate the wave  
687 with the settings used in `interFoam`. The tolerances on  $p^*$  (`pd`) needed to be reduced  
688 by a factor 100 and the tolerances on  $U$  (`U`) by a factor 10. Comparing the performance  
689 of the two is, however, still justified as `interFlow` actually, even with the decreased  
690 tolerances, performed the simulation slightly faster than `interFoam`. Moreover, the  
691 simulations with `interFoam` did not improve when lowering the tolerances with a  
692 factor 1000 as shown in Section 4.4. The speed-up in computational time was not due  
693 to larger time steps, but rather to the algorithm moving the free surface faster.

694 Figure 19 shows the surface elevations obtained utilizing the two different solvers. It  
695 is quite noticeable that, while with `interFoam` the wave heights start to increase, with  
696 `interFlow` the wave heights decrease mildly. Also shown are the contours for  $\alpha = 0.99$   
697 and  $\alpha = 0.01$  for the crest and trough for each period. Here it can be seen that the  
698 two contours are substantially closer with `interFlow`. They are constantly separated  
699 by less than two cell heights meaning that there is actually only one interface cell in  
700 the vertical direction. This is a substantial improvement of the surface representation  
701 compared to `interFoam`. Since equation (7) is not solved, there is no artificial com-  
702 pression term, and the interface wiggles previously observed are gone altogether. This  
703 is likewise a desirable improvement. The artificial compression term has been shown  
704 to have undesired effects, as it cause wiggles in the interface, in the simple propagation  
705 of a stream-function wave over sufficiently long propagation times. How these wiggles  
706 might behave in more complex situation like e.g. wave breaking is an open question,  
but one can imagine a greater effect in such a more chaotic situation.

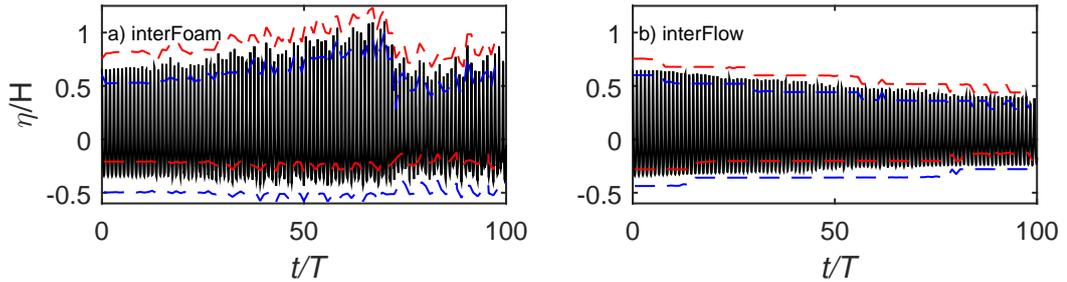


**Figure 19.** Simulated surface elevations (-) as a function of time utilizing `interFoam` and `interFlow` together with the  $\alpha = 0.99$  and  $\alpha = 0.01$  (- -) contours (Main fixed parameters:  $Co = 0.15$ ,  $N = 12.5$ , `ddt-Euler`, `grad-Gauss Linear`, `div(rho*phi,U)-Gauss LimitedLinearV 1`, `laplacian-Gauss linear corrected`).

707 In Figure 20 the velocity profile beneath the crest at  $t = 5T$  is shown utilizing  
708 both `interFoam` and `interFlow`. Here it is quite clear that `interFlow`, with the cur-  
709 rent settings is not improving the velocity profile. The crest velocity is slightly larger  
710 than the `interFoam` solution, and closer to the bed, the velocity is underestimated.  
711

This underestimation of velocity is probably due to the decrease in wave height. That

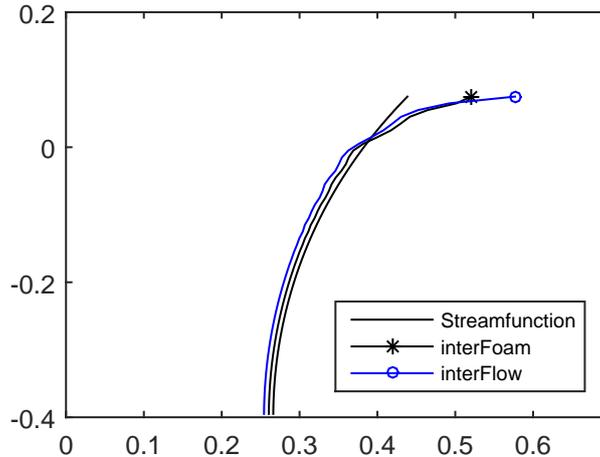


**Figure 20.** Velocity distribution beneath the crest at  $t = 5T$  utilizing `interFoam` and `interFlow` (Main fixed parameters:  $Co = 0.15$ ,  $N = 12.5$ , `ddt-Euler`, `grad-Gauss Linear`, `div(rho*phi,U)-Gauss LimitedLinearV 1`, `laplacian-Gauss linear corrected`).

712

713 `interFlow` gets an even larger error in the velocity in the top of the crest is proba-  
 714 bly due to the sharper interface, creating larger gradients, and any imbalance in the  
 715 momentum equation near the interface may then be increased.

716

As shown with `interFoam`, `interFlow` is also sensitive to the setup, and the same  
 717 diffusive balance that could be achieved with `interFoam` can also be achieved with  
 718 `interFlow`. In Figure 21 the simulated surface elevations utilizing `interFoam` and  
 719 `interFlow` respectively are once again compared, this time utilizing schemes to achieve  
 720 a diffusive balance. It can be seen that `interFlow`, like `interFoam`, is capable of  
 721 propagating the stream function wave for 100 periods, and that `interFlow` throughout  
 722 the simulation keeps a sharper interface as the  $\alpha = 0.01$  and  $\alpha = 0.99$  contours are  
 723 much closer. It can also be seen that `interFlow` does not have the same erratic surface  
 724 elevation when utilizing two outer correctors together with a blended CN scheme,  
 725 which can be explained by `interFlow` not having an artificial compression term, and  
 726 therefore the CN scheme does not excite any erratic behaviour near the free surface.  
 727 However like `interFoam`, `interFlow` is also very sensitive to the exact value of the  
 728 blended CN scheme, and lowering the blending factor, i.e. going more towards the  
 729 `Euler` scheme made the wave heights decay, and raising it towards more pure CN  
 730 made the wave heights increase.

731

The resulting velocity profiles are shown in Figure 22. Here it can be seen that  
 732 the two solvers perform quite similarly when utilizing an `upwind` scheme together  
 733 with a blended CN scheme, and that the overestimation of the velocity near the crest  
 734 is reduced. Furthermore, it can be seen that `interFlow` also shows a significantly  
 735 improved velocity profile when switching to two outer correctors, together with a  
 736 blended CN scheme and that `interFlow` does not suffer, to the same degree, from  
 737 oscillations in the velocity profile as did `interFoam`.

738

To further underline the impressive performance of `interFlow` when utilizing a  
 739 balanced setup, Figure 23 shows the surface elevation from the 95th to the 100th  
 740 period together with the velocity profile beneath the crest at  $t = 100T$ . Here it can be  
 741 seen that even after propagating the nonlinear wave for 100 periods `interFlow` still  
 742 follows the analytical stream function solution. The surface elevations are of the right  
 743 magnitude, and there are no significant phase differences. Furthermore, it can be seen

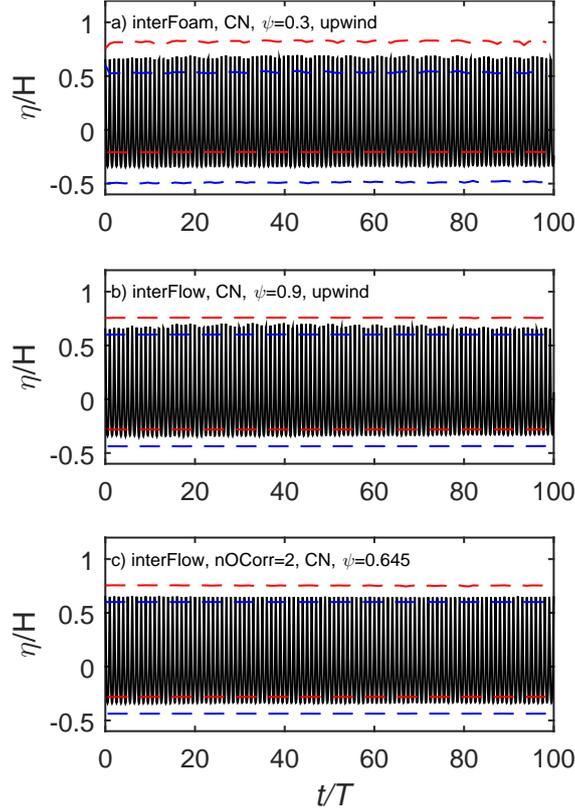


**Figure 21.** Simulated surface elevations (-) as a function of time utilizing `interFoam` and `interFlow` together with the  $\alpha = 0.99$  and  $\alpha = 0.01$  (- -) contours (Main fixed parameters:  $Co = 0.15$ ,  $N = 12.5$ , `grad-Gauss Linear`, `laplacian-Gauss linear corrected`).

744 that the velocity profile is likewise quite close to the analytical result, though it suffers  
 745 from minor oscillations.

## 746 6. Conclusions

747 In this study the performance of `interFoam` (a widely used solver in `OpenFOAM`) in  
 748 the simulation of progressive regular gravity waves (having intermediate depth and  
 749 moderate nonlinearity) has been systematically documented. It has been shown that  
 750 utilizing the basic settings of the popular `interFoam` tutorial `damBreak` will yield quite  
 751 poor results, resulting in increasing wave heights, a wiggled interface, spurious air  
 752 velocities, and severely overestimated velocities near the crest. These four problems  
 753 can be reduced substantially by lowering the time step and increasing the spatial  
 754 resolution. It has been shown that a rather small time step, corresponding to a Courant  
 755 number  $Co \approx 0.05$  is needed to give a good solution when propagating a wave even  
 756 short distances of around five wave wave lengths.

757 To test whether an improved solution could be achieved without (drastically) low-  
 758 ering the time step and increasing the spatial resolution, a set of simulation have been  
 759 performed, where the discretization schemes and iterative solution procedures were  
 760 changed one at a time. By gradually increasing and lowering the artificial compression  
 761 term ( $c_\alpha$ ), it was identified as root of the interface wiggles, which was exacerbated  
 762 when increasing the  $c_\alpha$  and damped or completely removed when lowering  $c_\alpha$ . It was

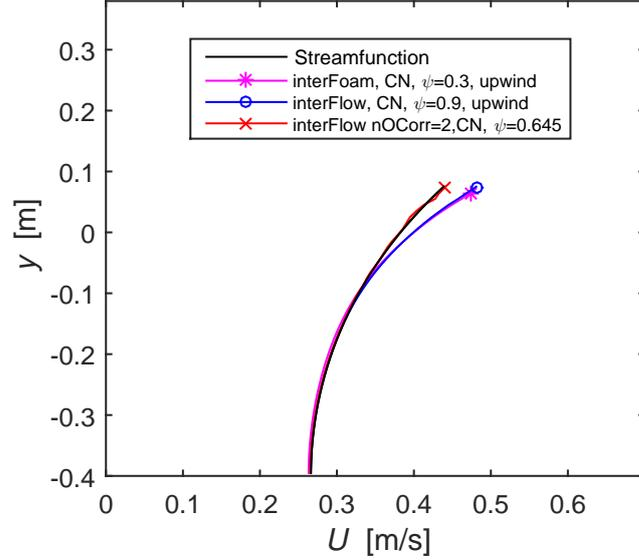


**Figure 22.** Velocity distribution beneath the crest at  $t = 5T$  utilizing an upwind scheme for the convection for `interFoam` with  $CN(\psi=0.3)$  as well as `interFlow` with  $CN(\psi=0.9)$  and two outer correctors with  $CN(\psi=0.645)$  (Main fixed parameters:  $Co = 0.15$ ,  $N = 12.5$ , `grad-Gauss Linear`, `laplacian-Gauss linear corrected`).

763 also shown how changing from first-order backward Euler time discretization scheme  
764 to the (almost) second order, and less diffusive, blended Crank-Nicolson scheme caused  
765 the wiggles to appear earlier and cover a larger part of the interface. The convection  
766 schemes was shown to affect not only the interface wiggles, but also the development of  
767 the wave heights as well as the velocities beneath the crest. More diffusive convection  
768 schemes removed the interface wiggles and delayed the increase in wave heights or in  
769 fact, when using an **upwind** scheme, caused the wave heights to decrease. Furthermore,  
770 the more diffusive schemes also reduced the overestimation of the crest velocities. In  
771 general the effect of the gradient schemes was not as large as the convection schemes,  
772 but the **fourth** scheme improved the solution, and the `faceMDLimited` scheme behaved  
773 very similar to the **upwind** convection scheme. Finally changing the `snGrad` scheme  
774 in the Laplacian created large spurious velocities in the air phase directly above the  
775 wave. These high velocities however did not seem to influence the wave kinematics.  
776 This was further backed by simulations done with a fixed time step, which clearly  
777 indicated that the spurious air velocities, while being an unwanted and un-physical  
778 phenomenon, do not have a large impact on the wave kinematics. By combining more  
779 or less diffusive schemes it was shown that a "diffusive balance" could be reached,  
780 where it was possible to propagate the wave a full 100 wave lengths while maintaining  
781 its shape. One of these balanced settings also showed a significant improvement in the  
782 velocity profile beneath the crest.

783 The new open source solver `interFlow` was subsequently applied, and it was shown  
784 that `interFlow` was capable of propagating the wave for 100 periods. The wave de-  
785 creased slightly in time, but the interface was a lot sharper, and the wiggles in surface  
786 disappeared. Regarding the velocity profile `interFlow` performed slightly worse than  
787 `interFoam` with the base settings. Finally it was shown that `interFlow` could achieve  
788 the same kind of diffusive balance which enabled the solver to propagate the wave for  
789 100 periods while maintaining it shape and also maintaining a good match with the  
790 analytical velocity profile.

791 Given its rapidly growing popularity among scientists and engineers, it is hoped that

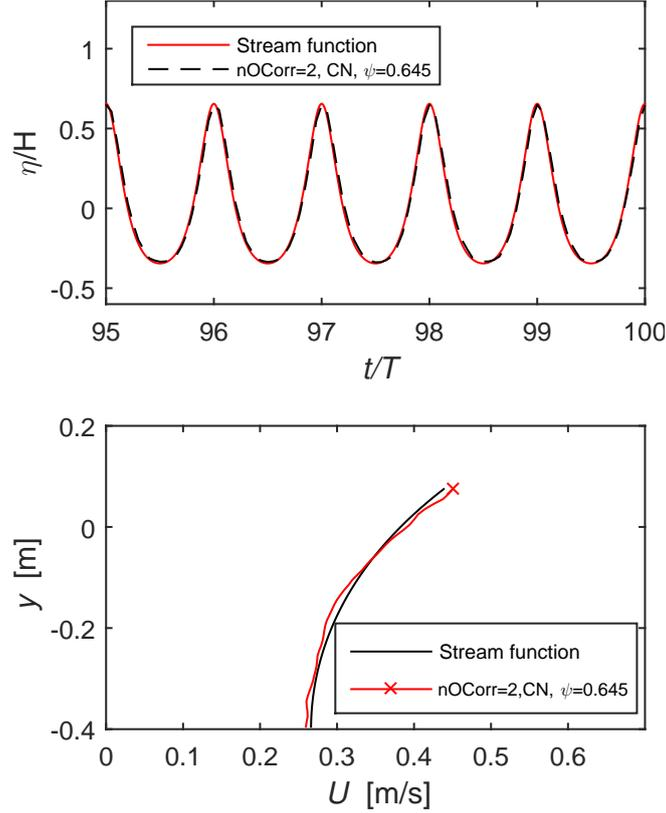


**Figure 23.** Surface elevations and velocity distribution beneath the crest after 100 periods utilizing interFlow.

792 the present systematic study will raise awareness and enable users to more properly  
 793 simulate a wide variety of problems involving the general propagation of surface waves  
 794 within the open-source CFD package `OpenFOAM`. While the present study has focused  
 795 on the canonical situation involving progressive non-breaking waves, the experience  
 796 presented herein is expected to be widely relevant to other, more general, problems  
 797 e.g. involving wave-structure interactions, propagation to breaking and resulting surf  
 798 zone dynamics, as well as boundary layer and sediment transport processes that result  
 799 beneath surface waves, all of which fundamentally rely on an accurate description of  
 800 surface waves and their underlying velocity kinematics.

## 801 Funding

802 The first two authors acknowledge support from the European Union project  
 803 `ASTARTE-Assessment, Strategy And Risk Reduction for Tsunamis in Europe`, Grant  
 804 no. 603839 (FP7-ENV-2013.6.4-3). The third author additionally acknowledges: `Sapere`  
 805 `Aude: DFF-Research Talent` grant from The Danish Council for Independent Re-  
 806 search — Technology and Production Sciences (Grant-ID: DFF - 1337-00118). The  
 807 third author also enjoys partial funding through the `GTS` grant to DHI from the  
 808 Danish Agency for Science, Technology and Innovation. We would like to express our  
 809 sincere gratitude for this support.

810 **References**

- 811 Afshar, M. A. (2010). Numerical Wave Generation in OpenFOAM. MSc Thesis, Chalmers  
 812 University of Technology Gotheburg, Sweden.
- 813 Brown, S. A., D. M. Greaves, V. Magar, and D. C. Conley (2016). Evaluation of turbulence  
 814 closure models under spilling and plunging breakers in the surf zone. *Coast. Eng.* 114,  
 815 177–193.
- 816 Chen, L. F., J. Zang, A. J. Hillis, G. C. J. Morgan, and A. R. Plummer (2014). Numerical  
 817 investigation of wave-structure interaction using OpenFOAM. *Ocean Eng.* 88, 91–109.
- 818 Deshpande, S. S., L. Anumolu, and M. F. Trujillo (2012). Evaluating the performance of the  
 819 two-phase flow solver interFoam. *Comput. Sci. Discov.* 5(1), article no. 014016.
- 820 Francois, M. M., S. J. Cummins, E. D. Dendy, D. B. Kothe, J. M. Sicilian, and M. W. Williams  
 821 (2006). A balanced-force algorithm for continuous and sharp interfacial surface tension  
 822 models within a volume tracking framework. *J. Comp. Phys.* 213(1), 141–173.
- 823 Galusinski, C. and P. Vigneaux (2008). On stability condition for bifluid flows with surface  
 824 tension: Application to microfluidics. *J. Comp. Phys.* 227(12), 6140–6164.
- 825 Greenshields, C. J. (2015). *OpenFOAM, The Open Source CFD Toolbox, Programmer’s Guide.*  
 826 *Version 3.0.1.* OpenFOAM Foundation Ltd.
- 827 Greenshields, C. J. (2016). *OpenFOAM, The Open Source CFD Toolbox, User’s Guide. Version*  
 828 *4.0.* OpenFOAM Foundation Ltd.
- 829 Higuera, P., J. L. Lara, and I. J. Losada (2013). Simulating coastal engineering processes with  
 830 OpenFOAM (R). *Coast. Eng.* 71, 119–134.
- 831 Hu, Z. Z., D. Greaves, and A. Raby (2016). Numerical wave tank study of extreme waves and  
 832 wave-structure interaction using OpenFoam (R). *Ocean Eng.* 126, 329–342.
- 833 Hysing, S. (2006). A new implicit surface tension implementation for interfacial flows. *Int.l J.*  
 834 *Numer. Meth. Fluids* 51(6), 659–672.
- 835 Jacobsen, N. G., J. Fredsøe, and J. H. Jensen (2014). Formation and development of a breaker  
 836 bar under regular waves. Part 1: Model description and hydrodynamics. *Coast. Eng.* 88,  
 837 182–193.
- 838 Jacobsen, N. G., D. R. Fuhrman, and J. Fredsøe (2012). A wave generation toolbox for the  
 839 open-source CFD library: OpenFOAM (R). *Int. J. Numer. Meth. Fluids* 70, 1073–1088.
- 840 Jacobsen, N. G., M. R. A. van Gent, and G. Wolters (2015). Numerical analysis of the  
 841 interaction of irregular waves with two dimensional permeable coastal structures. *Coast.*  
 842 *Eng.* 102, 13–29.
- 843 Larsen, B. E. and D. R. Fuhrman (2018). On the over-production of turbulence beneath  
 844 surface waves in Reynolds-averaged Navier-Stokes models. *J. Fluid Mech.* 853, 419–460.
- 845 Liu, Y. and O. Hinrichsen (2014). CFD modeling of bubbling fluidized beds using OpenFOAM  
 846 (R) : Model validation and comparison of TVD differencing schemes. *Computers and Chem.*  
 847 *Eng.* 69, 75–88.
- 848 Lupieri, G. and G. Contento (2015). Numerical simulations of 2-d steady and unsteady break-  
 849 ing waves. *Ocean Eng.* 106, 298–316.
- 850 Meier, M., G. Yadigaroglu, and B. L. Smith (2002). A novel technique for including surface  
 851 tension in plic-vof methods. *European J. Mech. B-fluids* 21(1), 61–73.
- 852 Menard, T., S. Tanguy, and A. Berlemont (2007). Coupling level set/VOF/ghost fluid methods:  
 853 Validation and application to 3D simulation of the primary break-up of a liquid jet. *Int. J.*  
 854 *Multiphase Flow* 33(5), 510–524.
- 855 Paulsen, B. T., H. Bredmose, H. B. Bingham, and N. G. Jacobsen (2014). Forcing of a bottom-  
 856 mounted circular cylinder by steep regular water waves at finite depth. *J. Fluid Mech.* 755,  
 857 1–34.
- 858 Popinet, S. and S. Zaleski (1999). A front-tracking algorithm for accurate representation of  
 859 surface tension. *Int. J. Numer. Meth. in Fluids* 30(6), 775–793.
- 860 Rienecker, M. and J. Fenton (1981). A fourier approximation method for steady water-waves.  
 861 *J. Fluid Mech.* 104(MAR), 119–137.
- 862 Roenby, J., H. Bredmose, and H. Jasak (2016). A computational method for sharp interface

863 advection. *Royal Society Open Science* 3(11), 160405.

864 Roenby, J., H. Bredmose, and H. Jasak (2017). Isoadvector: Geometric VOF on general meshes.

865 In *11th OpenFOAM Workshop*. 11th OpenFOAM Workshop. Springer Nature.

866 Roenby, J., B. E. Larsen, H. Bredmose, and H. Jasak (2017). A new volume-of-fluid method

867 in OpenFOAM. In *7th Int. Conf. Comput. Methods Marine Eng.*, pp. 1–12. 7th Int. Conf.

868 Comput. Methods Marine Eng. Nantes, France.

869 Rudman, M. (1997). Volume-tracking methods for interfacial flow calculations. *Int.l J. Numer.*

870 *Meth. Fluids* 24(7), 671–691.

871 Schmitt, P. and B. Elsaesser (2015). On the use of OpenFOAM to model oscillating wave

872 surge converters. *Ocean Eng.* 108, 98–104.

873 Shirani, E., N. Ashgriz, and J. Mostaghimi (2005). Interface pressure calculation based on

874 conservation of momentum for front capturing methods. *J. Comp. Phys.* 203(1), 154–175.

875 Tanguy, S., T. Menard, and A. Berlemont (2007). A level set method for vaporizing two-phase

876 flows. *J. Comp. Phys.* 221(2), 837–853.

877 Ting, F. C. K. and J. T. Kirby (1994). Observation of undertow and turbulence in a laboratory

878 surf zone. *Coast. Eng.* 24(1-2), 51–80.

879 Tomaselli, P. (2016). *Detailed analyses of breaking wave dynamics interaction with nearshore*

880 *and offshore structures*. Ph. D. thesis, . Technical University of Denmark., Kgs. Lyngby,

881 Denmark.

882 Vukcevic, V. (2016). *Numerical Modelling of Coupled Potential and Viscous Flow for Marine*

883 *Applications*. Ph. D. thesis, University of Zagreb, Zagreb, Croatia.

884 Vukcevic, V., H. Jasak, and I. Gatin (2017). Implementation of the ghost fluid method for free

885 surface flows in polyhedral finite volume framework. *Computers and Fluids* 153, 1–19.

886 Vukcevic, V., H. Jasak, and S. Malenica (2016). Decomposition model for naval hydrodynamic

887 applications, part i: Computational method. *Ocean Eng.* 121, 37–46.

888 Weber, J. (2016). Numerical Investigation on the Damping of Water Waves in a Towing Tank.

889 BSc. Thesis.Thechnical University of Berlin, Berlin, Germany. .

890 Wemmenhove, R., R. Luppens, A. E. P. Veldman, and T. Bunnik (2015). Numerical simula-

891 tion of hydrodynamic wave loading by a compressible two-phase flow method. *Comput.*

892 *Fluids* 114, 218–231.

893 Wroniszewski, P. A., J. C. G. Verschaeve, and G. K. Pedersen (2014). Benchmarking of navier-

894 stokes codes for free surface simulations by means of a solitary wave. *Coast. Eng.* 91, 1–17.